^{1}H MAS NMR Spectral Coalescence of Water and Hydroxyl Resonances in MCM-41

by

Jaspreet Walia

A thesis
presented to the University of Waterloo
in fullfillment of the
thesis requirement for the degree of
Master of Science
in
Physics

Waterloo, Ontario, Canada, 2011

I hereby declare that I am the sole author of this thesis. This is a true copy of the thesis, including any required final revisions, as accepted by my examiners.

_____

Jaspreet Walia

I understand that my thesis may be made electronically available to the public.

_____

Jaspreet Walia

Abstract

Solid state ^{1}H MAS NMR spectroscopy was used to investigate the temperature and hydration dependance of water and hydroxyl proton spectra of hydrated mesoporous MCM-41. The NMR spectra show a complex peak structure, with hydroxyl proton resonances seen in dry MCM-41 disappearing as water is introduced into the pores, and new peaks appearing representing water and hydrated silanol groups. Until now the assignment of these peaks was unclear and the consensus was that magnetization exchange played an important role in the coalescence of the various peaks which appear in the spectra. It was found recently that magnetization exchange is not necessary to produce the spectral featured observed [Niknam, M., M.Sc. Thesis, University of Waterloo (2010)].

In the present study a simplified model, based on chemical shift averaging by the making and breaking of hydrogen bonds as water undergoes rotational motion and translational self-diffusion on the pore surface, has been developed to explain the NMR spectral results. The model is able to reproduce the experimental ^{1}H MAS NMR spectra for all hydrations and temperatures studied. For the first time, definitive spectral assignments for all hydroxyl and water protons in the sample has been achieved. Spectral features arising due to temperature change have been explained by using the known result that the proton chemical shift of a hydrogen atom involved in hydrogen bonding varies linearly with temperature. Furthermore, it is reported for the first time, that with increasing hydration, water molecules begin to favour forming two hydrogen bonds to the surface. This may represent the first step in the pore filling process.

Acknowledgements

This work would have not been made possible without the tutelage and support of my supervisor Professor Hartwig Peemoeller. I learned many valuable lessons through his knowledge and wisdom of this world which surpass those of the everyday physicist. A true friendship was established here. There are no words to describe how much I appreciate the chance I was given to shine and reach my potential. Thank-you Professor Peemoeller.

I would also like to thank the imaging expert Dr. Claude Lemaire. He is the penultimate definition of a researcher. All of the experiments performed for this thesis were done under his guidance during which many laughs and interesting conversations were shared. He is another individual who has helped me reach my full abilities. Thanks Claude.

Table of Contents

List of Figures

List of Tables

CHAPTER 1

Introduction

The ability for water to form hydrogen bonds is responsible for many of its special physical properties. Water in confined geometries interacts with surfaces through hydrophobic and hydrophilic interactions, including hydrogen bond interactions. Thus, there is a competition between water-water interactions and water-surface interactions in these systems which can lead to interesting structures of water that are not observed in the bulk. For example, it is common to find some degree of ordering of the water molecules in zeolites, cements, or in the hydration shells of proteins. Recently, model systems with large surface areas and uniform pore structure such as the mesoporous material MCM-41 are being used in order to better understand the properties of water in confined geometries.

Even though the literature regarding the behaviour of water molecules in MCM-41 is considerable, controversy still remains concerning the details of the hydrated surface. Currently the details regarding the hydrogen bonding conformation of water molecules hydrogen bonded to the silanol surface as a function of hydration or temperature are not fully known. For example, the correlation times and residence timescales associated with water molecule motion, as well as accurate values for the diffusion coefficients as function of hydration are not fully defined at this time. In addition, the details concerning the pore filling process in MCM-41 are still debated.

Nuclear Magnetic Resonacne (NMR) is considered to be a powerful non-invasive tool to

investigate interactions of water with the hydroxyl groups of MCM-41. In MCM-41 hydration studies it has been found that the surface OH resonances seen in the 1-4 ppm region in dry MCM-41 are no longer visible in this ppm range for hydration levels above 0.2 monolayers. In other nano-porous materials such as zeolite or wood it has been shown that chemical exchange of magnetization between water and surface hydroxyl group protons is partially responsible for the observed chemical shift positions of resonance lines in ^{1}H Magic Angle Spinning (MAS) spectral data[2]. A reasonable explanation for the apparent disappearance of the surface OH resonances observed in dry MCM-41 is that with increasing hydration level they coalesce with the water resonance as a result of chemical exchange between water and surface OH hydrogens. Recently such exchange was quantified and its role in the coalescence of resonances and the disappearance of the OH resonances at low ppm values was discussed[1]. It was found that magnetization exchange was not needed for the coalescence of the resonances. The rate required for the resonances to coalesce is roughly two orders of magnitude larger than the experimentally determined rate of 300 s^{-1}. An alternate, more realistic model, involving time averaged chemical shift changes in both the water and OH group resonances, produced by the making and breaking of hydrogen bonds as water molecules diffuse on the MCM-41 pore surface and visit OH groups, was also intially proposed[1][3].

The objective of this research is to perform ^{1}H MAS NMR experiments over a range of temperatures (200-325 K) and hydrations (0-0.2 monolayers) and apply a chemical shift averaging model to the data. The prediction of the spectra by the model will confirm that magnetization exchange is not needed to explain hydrated MCM-41 spectra at the temperatures and hydrations studied. Furthermore, the model sheds light on water molecule surface interactions (water coordinations, pore filling, translational motion) in the MCM-41 material.

The basic theory behind magnetic resonance is given in Chapter 2 with details pertaining to dipole-dipole and quadrupolar interactions, magnetization exchange, and chemical shift. The structure, synthesis, and characterization of the MCM-41 nanomaterial is described in detail in Chapter 3. Water is described in Chapter 4 with focus on water-silica systems and existing research in this field. Details regarding the sample preparation and experimental NMR are given in Chapter 5. Chapter 6 contains the ^{1}H MAS NMR results, the model for chemical shift averaging through water molecule dynamics, and corresponding discussions. Conclusions and recommendations for future work are discussed in Chapter 7.

CHAPTER 2

Nuclear Magnetic Resonance

Introduction

In 1946, Felix Bloch and Edward Purcell discovered that when certain nuclei where placed in a magnetic field of a given strength they could absorb radio frequency (RF) energy specific to the identity of the nuclei. They were awarded the Nobel Prize for NMR in condensed matter for their discovery. The frequency of absorption is known as the *resonance* frequency. Specifically NMR is possible if the nucleus in question possesses a non-zero spin angular momentum, and a dipole magnetic moment,

$$\vec{\mu} = \gamma \hbar \vec{I} \qquad 2.1$$

where $\vec{I}$ is a dimensionless angular momentum operator, $\hbar$ is the reduced Planck's constant and γ is the gyromagnetic ratio. When such a nucleus is placed in a static magnetic field $\vec{B} = B_o \hat{z}$ it will experience a torque causing a precession about the z axis at an angular frequency

$$\omega_o = \gamma B_o \tag{2.2}$$

The interaction energy of a nucleus with $\vec{B}$ can be obtained using the following Hamiltonian, also known as the Zeeman Hamiltonian.

$$H_Z = -\vec{\mu} \cdot \vec{B} = -\gamma \hbar B_o I_z \tag{2.3}$$

The eigenvalues of this Hamiltonian, the allowed energies, are given by multiples of $\gamma \hbar B_o$

$$E_m = -\gamma \hbar B_o m \qquad m = I, I-1, \ldots, -I \tag{2.4}$$

For the case of $I = 1$ the energy levels are illustrated in Fig 2.1 which is the case for nuclei such as deuterons for example.

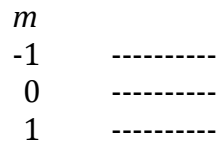

Fig 2.1: Nuclear Zeeman energy level diagram for $I = 1$. The spacing between levels is equal and is given by $\gamma \hbar B_o$.

In most NMR experiments one is typically observing the collective behaviour of an ensemble of nuclei at a given temperature T. These nuclei populate the energy eigenstates according to Boltzmann statistics. Consequently there is a slightly higher population of nuclear spins oriented parallel rather than anti-parallel to the static field B_o. Even though

the ratio of populations is close to unity the resulting net magnetization along the direction of B_o is detectable by NMR. The net magnetization M resulting from a volume density of N magnetic dipole moments per unit volume is given by Curie's Law,

$$M = \frac{N}{3\mathrm{k}_B T} \gamma^2 \hbar^2 I(I+1) B_o = \chi_o B_o \tag{2.5}$$

where k_B is the Boltzmann constant, and χ_o is the Curie susceptibility. In order to induce a significant number of transitions between nuclear Zeeman levels a perturbation in the form of a radio frequency (RF) field is applied along an axis perpendicular to B_o at the resonance frequency, that is

$$\omega = \omega_o = \gamma B_o \tag{2.6}$$

If we take the static field to be along the z-axis the RF perturbation can be written as

$$H_1 = -\gamma \hbar B_1 I_x \cos \omega_o t \tag{2.7}$$

As a result nuclei populating lower energy states can absorb energy from B_1 and populate higher energy states. The magnetization now also has components in the transverse plane.

2.1 The Bloch Equations

As described earlier the sample containing a spin volume density in a magnetic field will contain a dipole moment that experiences a torque and precesses at a frequency $\omega_o = -\gamma \vec{B}_o$. The time evolution of $\vec{M} = (M_x, M_y, M_z)$ inside $\vec{B}_0$ and under the influence of relaxation processes was first described by a set of phenomenological equations known as the Bloch equations[4]:

$$\frac{dM_x}{dt} = \gamma (M_y B_o + M_z B_1 \sin \omega t) - \frac{M_x}{T_2} \tag{2.8}$$

$$\frac{dM_y}{dt} = \gamma (M_z B_1 \cos \omega t + M_x B_o) - \frac{M_y}{T_2} \tag{2.9}$$

$$\frac{dM_x}{dt} = \gamma (M_x B_1 \sin \omega t + M_y B_1 \cos \omega t) - \frac{M_z - M_o}{T_1} \tag{2.10}$$

Two characteristic times describing two different relaxation processes appear in the above coupled ODEs. In a typical pulsed NMR experiment an application of a 90° RF pulse results in a net magnetization in the x-y plane. After the pulse has been turned off this magnetization experiences a loss of phase coherence due to spin-spin relaxation in a characteristic time T_2. Spin-lattice relaxation is the process that involves the spin ensemble returning to thermal equilibrium with time constant T_1 after being perturbed by

RF pulse. In almost all cases $T_2 < T_1$. The *lattice* in this case represents all non-spin degrees of freedom such as molecular motion. The loss of phase coherence manifests itself as a decaying signal which is due to freely precessing spins and hence the signal is commonly referred to as a free induction decay (FID) which allows for the determination of T_2.

2.2 Nuclear Spin Relaxation

Since the Bloch equations only describe the time evolution of the magnetization it is necessary to model the relaxation times T_1 and T_2 in terms of the physical details which describe the spin containing molecules both structurally and dynamically. It is well known that nuclei obey Quantum Mechanics and as such the first step in this connection is to introduce the nuclear spin Hamiltonian. For a spin system to relax back to thermal equilibrium resonant energy transitions must be induced between the spin states of the nuclei. These transitions are driven by fluctuating electromagnetic fields produced at the site of a particular nucleus by neighbouring nuclei as the molecules containing these nuclei undergo molecular motion. If the fluctuations contain frequency components that match the resonance condition of the nuclei involved then transitions can occur. In general, the relaxation rates are inversely proportional to the probability of such transitions. The probability itself depends on the type of interaction which is responsible for the transitions. For example for $I = 1/2$ the dominant intermolecular interaction causing

relaxation is the dipole-dipole interaction whereas for $I=1$ the main relaxation mechanism involved is based on the interaction of the nuclear electric quadrupole moment with the electric field gradient at the site of the nucleus.

2.2.1 Dipole-dipole Interaction

In system of spin 1/2 nuclei, the dipole-dipole interactions will be the dominant mechanism involved in relaxation processes. Each pairwise interaction between any two given spins depends on the magnitude of the individual magnetic moments as well as the separation vector describing their relative orientation with respect to the static field. As a result the probability that a transition will occur is strongly dependant on the relative motions of each nucleus being considered.

In order to ascertain the form of the dipolar Hamiltonian, H_D, it is useful to consider the classical energy of interaction between N pairs of magnetic moments μ_j and μ_k. This energy is given by

$$H_D = \frac{1}{2}\sum_{j=k}^{N}\sum_{j\neq k=1}^{N}\left[\frac{\vec{\mu}_j\cdot\vec{\mu}_k}{r_{jk}^3} - \frac{3(\vec{\mu}_j\cdot\vec{r}_{jk})(\vec{\mu}_k\cdot\vec{r}_{jk})}{r_{jk}^5}\right] \qquad 2.11$$

where $\vec{r}_{jk}$ is the separation vector between two pairs of spins. The quantum mechanical form is readily obtained by writing $\vec{\mu}$ in terms of the nuclear spin raising and lowering

operators,

$$I^{+} = I_x + iI_y \tag{2.12}$$

$$I^{-} = I_x - iI_y \tag{2.13}$$

and transforming from Cartesian to spherical polar coordinates. What results is a more convenient form for H_D [5],

$$H_D = \frac{\gamma_1 \gamma_2 \hbar^2}{r^3}\left(A + B + C + D + E + F\right) \tag{2.14}$$

where

$$A = I_{1z} I_{2z}\left(1 - 3\cos^2\theta\right)$$

$$B = \frac{\left(I_1^{+} I_2^{-} + I_1^{-} I_2^{+}\right)\left(3\cos^2\theta - 1\right)}{4}$$

$$C = -\frac{3}{2}\left(I_1^{+} I_{2z} + I_{1z} I_2^{+}\right)\sin\theta\cos\theta\, e^{-i\phi}$$

$$D = -\frac{3}{2}\left(I_1^{-} I_{2z} + I_{1z} I_2^{-}\right)\sin\theta\cos\theta\, e^{i\phi}$$

$$E = -\frac{3}{4} I_1^{+} I_2^{+}\sin^2\theta\, e^{-2i\phi}$$

$$F = -\frac{3}{4} I_1^{-} I_2^{-}\sin^2\theta\, e^{2i\phi}$$

Here θ is the angle formed between the internuclear vector connecting spins I_1 and I_2, and the main field B_o. The terms A, B, C, D, E, and F can be illustrated graphically using a Slichter diagram as shown in Figure 2.1. The A term is purely diagonal and connects the

states $|m_1 m_2\rangle$ and $\langle m_1 m_2|$. The B term connects the state $|m_1 m_2\rangle$ to the states $\langle m_1 \pm 1, m_2 \mp 1|$. Both A and B terms correspond to energy conserving transitions and therefore $\Delta E = 0$. The C and D terms flip only one spin and as such connect states that differ in energy by $\Delta E = \pm \hbar \omega$, whereas the E and F terms connect states that are $\Delta E = \pm 2 \hbar \omega$ apart in energy.

2.2.2 Relaxation times and correlation functions in aqueous solutions

Macroscopic NMR parameters such as T_1 and T_2 can be connected with molecular motions that exist in a liquid via time correlation functions $G(\tau)$. In general the relaxation rates are proportional to a linear combination of spectral density functions, $J(\omega_k)$, which are the Fourier transforms of the time correlation function.

$$J(\omega) = \int_{-\infty}^{\infty} G(\tau) e^{-i\omega\tau} d\tau \qquad 2.15$$

$$G(\tau) = \frac{1}{2\pi} \int_{-\infty}^{\infty} J(\omega) e^{i\omega\tau} d\omega \qquad 2.16$$

For a stationary process the correlation function corresponding to a random perturbation in time is written as[1]

$$G_{mn}(\tau) = \overline{\langle m|H_1(t-\tau)|n\rangle \langle n|H_1(\tau)|m\rangle} \qquad 2.17$$

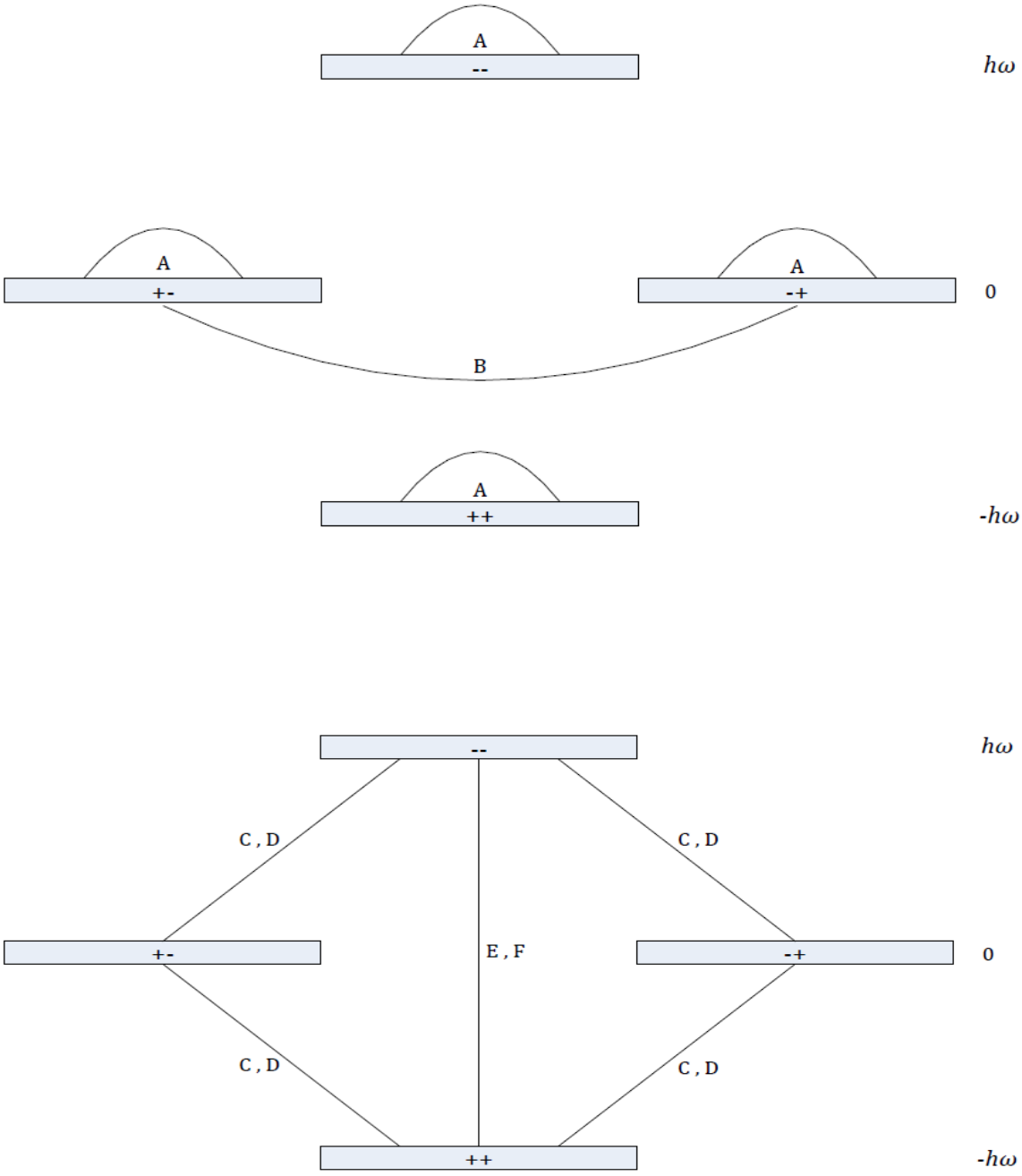

Fig 2.2: Slichter diagrams illustrating the states joined by the terms A, B, C, D, E, and F appearing in the dipolar Hamiltonian.

As an example, consider the case of dipolar coupling which was discussed in the previous section. The polar coordinates (r,θ,ϕ), which describe the orientation of the intermolecular vectors are time dependent as the molecules tumble with respect to the main field H_0. The orientational dependance can be described by the spherical harmonics of second order:

$$Y_{20}=\frac{1}{4}\sqrt{\frac{5}{\pi}}(3\cos^2\theta-1)$$

$$Y_{21}=\frac{-1}{2}\sqrt{\frac{15}{2}\pi}\sin\theta\cos\theta e^{i\phi} \qquad 2.18$$

$$Y_{22}=\frac{-1}{4}\sqrt{\frac{15}{2}\pi}\sin^2\theta e^{2i\phi}$$

For a Markoffian process the correlation function is

$$G(\tau)=G(0)e^{|\tau|/\tau_c} \qquad 2.19$$

where τ_c is the characteristic time for which the correlation between H_1 at one time and H_1 at a time τ later has decreased to $1/e$ of the maximum value $G(0)$. Performing the Fourier transform yields the following Debye form for the spectral density function,

$$J(\omega)=\overline{Y^2_{2m}(t)}\frac{1}{r^6}\frac{2\tau_c}{1+\omega^2\tau_c^2} \qquad 2.20$$

In 1948, Nicolass Bloembergen, Edward Purcell, and Robert Pound proposed the BPP theory which explains the relaxation behaviour of a pure substance[6]. This theory takes into account the tumbling motion of molecules and their effects on the local magnetic field. The theory assumes a Markoffian process from which one can obtain equations for T_1 and T_2 for magnetic dipolar relaxation. The BBP expressions for two like-dipoles with constant separation distance become

$$\frac{1}{T_1}=\beta\left\{\frac{\tau_c}{1+\omega^2\tau_c^2}+\frac{4\tau_c}{1+4\omega^2\tau_c^2}\right\} \tag{2.21}$$

$$\frac{1}{T_2}=\frac{\beta}{2}\left\{3\tau_c+\frac{5\tau_c}{1+\omega^2\tau_c^2}+\frac{2\tau_c}{1+4\omega^2\tau_c^2}\right\} \tag{2.22}$$

Here β is a constant defined by

$$\beta=\frac{3\mu^2\hbar^2\gamma^4}{160\pi^2 r^6} \tag{2.23}$$

with μ being the magnetic dipole moment of the spins.

If one assumes an Arrhenius type of behaviour for τ_c,

$$\tau_c=\tau_0 e^{\frac{E_a}{k_B T}} \tag{2.24}$$

In the high temperature limit the condition of extreme motional narrowing is encountered, $\omega_0\tau_0 \ll 1$ and $T_1 = T_2$. As the temperature decreases (motional narrowing regime), $\omega_0\tau_c > 1$ and T_1 becomes greater than T_2. In the rigid-lattice regime $\omega_0\tau_c \gg 1$. Here the molecular motion is slower than T_2 and the relaxation time T_2 becomes independent of temperature.

2.2.3 Quadrupolar Interaction

More than 70% of the nuclei in the periodic table have a spin $I \geqslant 1$ along with a non-spherically symmetric charge distribution and a quadrupolar moment. The main interaction is between the electric quadrupole moment, eQ, and the electric field gradient produced at the site of the nucleus by the surrounding electrons.

If one considers a principal axes system for which all off-diagonal elements of the electric field gradient tensor vanish, then only the diagonal components of the electrostatic potential, V_{xx}, V_{yy}, and V_{zz} remain. The quadrupolar Hamiltonian can then be written as[7],

$$H_Q = \left(\frac{e^2qQ}{4\mathrm{I}(2\mathrm{I}-1)}\right)\left(3\mathrm{I}_z^2 - I^2 + \frac{1}{2}\eta\left(I_+^2 + I_-^2\right)\right) \qquad 2.25$$

where $eq = V_{zz}$ is the maximum component of the electric field gradient and η is known as the asymmetry parameter defined by

$$\eta = \frac{V_{xx} - V_{yy}}{V_{zz}} \qquad 2.26$$

The deuterium nucleus has a spin $I = 1$ and its gyromagnetic ratio is 6.5 times smaller than that of the hydrogen nucleus. In a typical ^{2}H NMR experiment , the dipolar interactions and chemical shift dispersions are quite often neglected. The reason for this being that the ^{2}H-^{2}H and the ^{2}H-^{1}H dipolar couplings are both negligible relative to the quadrupolar interaction strength (~250 kHz) and the chemical shift dispersion is only about 1 kHz[1]. The advantage of this is that the deuteron can essentially be treated as an isolated spin-1 nucleus making it an excellent probe for studies involving intramolecular motion.

2.3 Chemical Shift

As is well known from classical electrodynamics, a nucleus in the region of a changing magnetic field will have its electrons circulate in such a manner as to oppose the change in the magnetic field causing the actual value of magnetic field at the nucleus to vary. Subsequently atoms with higher electron density are called shielded relative to those with lower electron density. The degree of shielding of a particular nucleus is called the chemical shift. In the case of hydrogen bonded nuclei, for example, the electron donor becomes deshielded and the electron acceptor becomes more shielded due to the resulting

increased electron density.

The NMR chemical shift allows for distinguishing identical nuclei within a given molecule. Since nuclei in all molecules are never isolated from charged electrons which are in motion, the magnetic field at the nucleus takes on a slightly different value than that of the main applied field. The difference can be represented as a fraction of the main field. This quantity is referred to as the chemical shift and for protons is usually in the parts per million (ppm) range. Chemical shift is usually expressed in parts per million by frequency and can be expressed as follows

$$\delta = \frac{\nu - \nu_{ref}}{\nu_0} \tag{2.27}$$

Since the observed chemical shift depends on the orientation of the molecule with respect to the main field, the NMR chemical shift is actually a tensor quantity. In diagonalized matrix form the tensor can be written as,

$$\boldsymbol{\delta} = \begin{pmatrix} \delta_{11} & 0 & 0 \\ 0 & \delta_{22} & 0 \\ 0 & 0 & \delta_{33} \end{pmatrix} \tag{2.28}$$

Here the components δ_{11} , δ_{22} , and δ_{33} are the components of the chemical shift tensor in a principal axis system. In a powder sample one would observe the three principal components. The 11 and 33 components are the highest and lowest chemical shifts respectively and therefore would represent the wings appearing in a powder spectrum for example. The 22 component is the most likely orientation and would be seen as the most

intense portion of the spectrum. In solution NMR the molecules are tumbling rapidly with respect to the main field and one generally observes an average isotropic value of the tensor given by.

$$\delta_{isotropic} = \frac{1}{3}(\delta_{11} + \delta_{22} + \delta_{33}) \qquad 2.29$$

From a physics perspective the chemical shift is ultimately quantum mechanical and electrodynamic in origin and arises due to nuclear shielding, which is also a tensor quantity. Specifically this quantity is referenced directly to the bare nucleus and therefore is an absolute quantity. The chemical shift goes in an opposite direction to that of nuclear shielding and is usually measured with respect to a reference sample. This sample is usually a molecule which has an electron cloud which is minimally distorted. In the case of ^{1}H and ^{13}C NMR the reference sample is usually tetramethylsaline (TMS) or 4,4-dimethyl-4-silapentane-1-sulfonic acid (DSS) since the protons on these molecules absorb RF energy at the same frequencies. A chemical shift of zero is generally assigned to the reference samples to which all subsequent measurements of chemical shift are referenced. Chemical shift is just a measure of how much a nucleus has become shielded or deshielded and therefore the theory regarding the calculation of nuclear shielding constants is of importance. In terms of the nuclear shielding tensor itself, the 11 component is the least shielded (highest chemical shift), the 33 component is the most shielded (lowest chemical shift).

Nuclear shielding from a quantum mechanical perspective is defined formally as the mixed second derivative of the energy with respect to the magnetic moment of the nucleus, and the strength of the applied field. The solutions are obtained using second-order perturbation theory[5]. The contribution due to the first order correction is called diamagnetic while the second-order contribution is called paramagnetic. In order to obtain the second-order contribution one requires knowledge of the excited electronic states.

It is now commonplace for NMR laboratories to have access to powerful workstations or even supercomputers in some cases to calculate NMR chemical shifts. The latest methods employed are ab-initio post Hartee-Fock calculations. These methods essentially improve the Hartee-Fock method by taking into account the effects of electron correlations. The Hartee-Fock method assumes that a single Slater determinate can approximate an entire *N*-body wavefunction of the entire system. In general, the solutions to many-electron systems do not exist at all and the problem is solved numerically using a non-linear iterative approach. As such the Hartee-Fock method is a self consistent field theory. Typically the one electron wavefunctions are modelled as a linear combination of atomic orbitals (referred to as LCAO in quantum chemistry discussions). Specifically according to the theory the orbitals are Slater-type orbitals[8], however in the interests of saving extremely large amounts of computation time the orbitals are actually composed of a linear combination of one or more Gaussian-type orbitals (GTOs). The reason why using Gaussian basis sets in quantum chemical calculations can save computational expense is due to the Gaussian product theorem[9]. This theorem states that the product of any two Gaussian-type orbitals centered on any two atoms becomes a finite sum of Gaussian-type

orbitals which is centered along the axis connecting the two atoms. The significance here is that for example four GTOs centered on four different atoms can be reduced to a finite sum of Gaussians centered on the same point. This results in a decrease of computation time by about five orders of magnitude compared to when Slater-type orbitals are employed. As such most software packages that calculate NMR shielding parameters employ Gaussian basis functions to fit the electronic orbitals in a molecule. The calculations generally yield the tensor quantity and its components and the accuracy increases with the number of Gaussians used.

The non-experimental chemical shifts calculated by other researchers which appear later (Chapter 6) were done so using the computational methods described above. Similar calculations were performed for this thesis using the Spartan 08 software environment. However none of the results of the ab-initio calculations performed were used in the writing of this work.

2.4 Exchange Processes In NMR

The concept of magnetization exchange in NMR can refer to physical, chemical or magnetic exchange. In most solid state NMR experiments the sample being studied contains spin groups in different physical environments having various spectral and relaxation characteristics. Magnetic exchange can occur between spins in these groups via

spin flip-flops for example (see section 2.2.1). Chemical exchange involves processes in which an atom exchanges between two sites as chemical bonds are being broken and reformed or processes in which exchange between different conformations of a molecule occur. It is important to note that the timescales associated with chemical exchange and translational diffusion can overlap in certain cases. This goes to say that on the second to microsecond timescales both motional and chemical exchange are the two important processes which need to be considered.

As an example the physical basis for two site magnetization exchange will follow. Consider two spin groups *a* and *b* from two different environments, which are exchanging their magnetizations M_a and M_b with each other. The time evolution of the magnetization is given by the following pair of coupled differential equations[1].

$$\frac{d}{dt}\begin{pmatrix} M_a \\ M_b \end{pmatrix} = \begin{pmatrix} R_{11} & R_{12} \\ R_{21} & R_{22} \end{pmatrix}\begin{pmatrix} M_a \\ M_b \end{pmatrix} \qquad 2.30$$

where

$$R_{11} = -R_a - k_{ab}$$

$$R_{12} = k_{ba}$$

$$R_{21} = k_{ab}$$

Here *R* is the relaxation rate which is the inverse of T_1 or T_2 The exchange rates k_{ab} and k_{ba} represent the rate of exchange of magnetization from one site to another. Additionally these rate processes satisfy the detailed balance equation $M_{a_o} k_{ab} = M_{b_o} k_{ba}$. The solutions to the above differential equations are given elsewhere[1][3]. The final answer has the form

$$\begin{pmatrix} M_a \\ M_b \end{pmatrix} = \frac{1}{1-\alpha\beta}\begin{pmatrix} e^{\lambda_+ t} - \alpha\beta\, e^{\lambda_- t} & \beta\left(e^{\lambda_- t} - e^{\lambda_+ t}\right) \\ \alpha\left(e^{\lambda_+ t} - e^{\lambda_- t}\right) & e^{\lambda_- t} - \alpha\beta\, e^{\lambda_+ t} \end{pmatrix}\begin{pmatrix} M_{a_o} \\ M_{b_o} \end{pmatrix} \qquad 2.31$$

With

eigenvalues,

$$\lambda_{\pm} = \frac{\left(R_{11}+R_{22}\right) \pm \sqrt{\left(R_{11}-R_{22}\right)^2 + 4R_{12}R_{21}}}{2}$$

and,

$$\alpha = \frac{\lambda_+ - R_{11}}{R_{12}}$$

$$\beta = \frac{\lambda_- - R_{22}}{R_{21}}$$

The time evolution of the magnetization for each spin is now given by the two uncoupled equations in equation 2.31.

CHAPTER 3

MCM-41

Introduction

Mesoporous silicas are a form of silica nanostructures that are well known for their high surface areas and tuneable pore sizes. These porous materials play an important role in a wide range of disciplines and have recently been researched extensively for use in the catalysis industry. Additionally scientists are interested in the applications of mesoporous silicas for use in soil and water treatment systems, bio-sensors, and nano drug delivery devices.

Mesoporous materials also present themselves as model systems in which to study the behaviour of fluids in confined geometries. For example water confined in porous materials experiences a depression in its freezing point thus allowing for measurements on supercooled water to be made in the so called “no man's land” region of the temperature scale for water.

In 1992 a group of researchers at Mobil Oil reported a new family of mesoporous silica based materials denoted as M41S[10][11]. Mobil Composition of Materials number 41 (MCM-41) is one member of this family. MCM-41 is synthesized using rod-like micelles of cationic surfactant as a template. The material itself is composed of amorphous silica and possesses uniform hexagonal pores which can be varied from 20 to 100 A° in diameter as well as high BET surface areas (~1000m^2/g). An exhaustive review of this material can be found in[12].

3.1 MCM-41 Surface Chemistry

There are four different silanol (SiOH) groups in MCM-41 [13] denoted as Q^{4-n}, where *n* represents the number of hydroxyl (OH) groups bonded to a silicon atom. For example in a Q^4 group, silicon is bonded to four oxygen atoms which in turn are bonded to silicon atoms. This group is mainly located within the pore walls. Q^2 is commonly referred to as a geminal group which has two hydroxyl groups attached to the silicon. This group makes up a very small fraction (2-5%) of the silanol groups present in MCM-41 (Figure 3.1). The most abundant silanol group is the Q^3 group (40-60%). Here the silicon has only one hydroxyl group attached to it. The Q^3 hydroxyl groups can either exist as single, $(SiO)_3$Si-OH, or hydrogen bonded, $(SiO)_3$Si-OH-OH-Si$(SiO)_3$ groups and are found on the pore surfaces of MCM-41. The density of surface silanol groups in MCM-41 varies between 2.5-5 nm^{-2} [1] and the number of single and hydrogen bonded hydroxyl groups can be varied with

temperature. It has been shown that heating MCM-41 to ~680 K removes the hydrogen bonded groups[12][13], and upon further heating the material to~800 K [14] forces the single silanol groups to dehydrate (Figure 3.1).

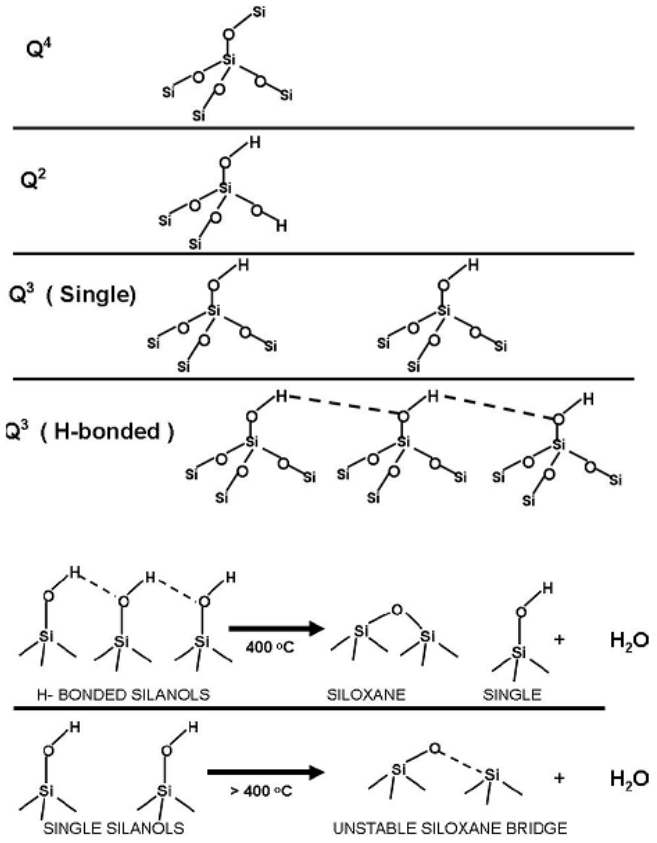

Fig 3.1: The different Q^n silanol groups in MCM-41 (top) and the effect of thermal energy on single and hydrogen bonded hydroxyl groups (bottom)[14][17].

3.2 MCM-41 Synthesis

Mesoporous MCM-41 can be synthesized using a variety of methods. A basic schematic representation of the formation of MCM-41 is shown in Figure 3.2. In addition to a silica source, all the procedures have in common the requirement for a templating agent. These structure-directing agents usually are made up relatively simple molecules around which a frame work is built up. For the synthesis of MCM-41 quaternary ammonium ions are frequently used. To minimize energetically unfavourable interactions between the apolar alkyl chains (C_nH_{2n+1}) and the polar water molecules, the template ions aggregate together to form micelles. The large alkyl chains are contained within the hydrophobic core of the micelles and by altering the length of the alkyl chains involved during synthesis one can vary the pore diameter from ~ 20 to 100 Å. Spherical micelles are the most energetically favourable form of micelles since this conformation allows the surface energy to be minimized most efficiently. Additionally the spherical geometry allows for the largest number of micelles to be formed from a given quantity of surfactant. However, it is observed that as the template head to tail ratio is changed, new micelle geometries evolve. The spherical micelles gradually begin to transform into rod-like micelles and upon further increasing the template concentration the rod-like micelles aggregate into hexagonal liquid crystalline units which resemble the MCM-41 structure.

Besides a structure directing agent, water, and a source of silica, a mineralizing agent is required for the dissolution of the silica source which produces silicate anions. Due to electrostatic interactions the silicate anions diffuse towards the surfaces of the rod

like micelles. As the concentration of anions at the micelle surface increases they begin to condense into a monolayer at the micelle surfaces. At this stage the silica coated rod-like micelles begin to aggregate, generating the hexagonal MCM-41 network (figure 3.2). As a result of these processes the pore walls of MCM-41 are amorphous by nature and only two to three monolayers thick[14]. The final process in the synthesis involves calcination of the product to remove the template material. During this process the template is decomposed into CO_2, NO_2, and steam.

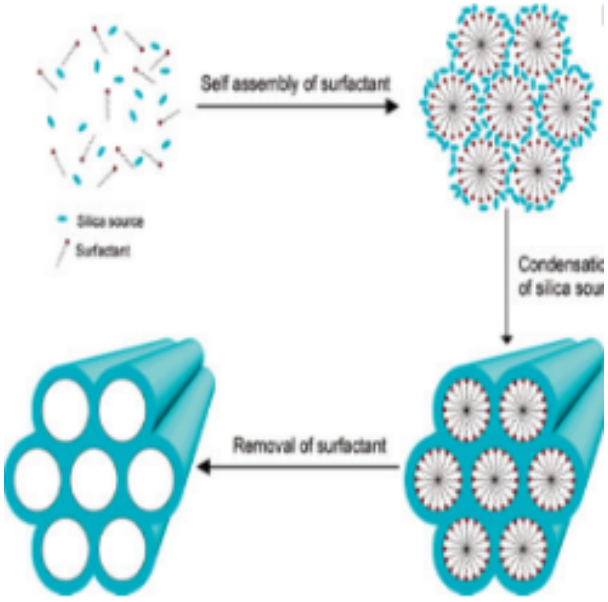

Fig 3.2: Schematic representation of the formation of MCM-41[18].

3.4 MCM-41 Characterization

The pore size distribution and specific surface area of MCM-41 can be determined using nitrogen adsorption measurements. The technique involves analyzing the amount of N_2 gas adsorbed onto the surfaces of a given sample versus pressure. The resulting data set is commonly referred to as a *nitrogen adsorption isotherm* and is analyzed using the BET model (named after the researchers Brunauer, Emmett and Teller[19]). A typical BET isotherm is fitted to the following equation[1]

$$\frac{P}{V(P_o - P)} = \frac{1}{V_m C} + \frac{C-1}{V_m C}\frac{P}{P_o} \qquad 3.1$$

Here V is the volume of gas adsorbed, V_m is the volume of gas corresponding to a monolayer, P_o is the saturating vapor pressure of the gas. The above equation can be used to determine the specific surface area of a given material[20][21]. For example MCM-41 synthesized from Aldrich chemical company has a BET surface area of ~1000 m^2/g. Additionally from the experimental nitrogen adsorption data one can determine the pore size distribution using the Kelvin

equation.[20]

Mesoporous silicas are generally in the form of a polycrystalline powder which requires an x-ray powder diffraction experiment to be performed in order to gain insight into the atomic ordering present. In an ideal sample every possible crystalline orientation is sampled equally. Powder diffraction data are represented as a *diffractogram* which

displays scattering intensity as a function of the scattering angle 2θ. A detailed explanation of XRD is beyond the scope of this thesis and is treated elsewhere[22][23]. The MCM-41 powder diffractogram shows well resolved peaks which are characteristic of the highly ordered hexagonal pattern[24]. The diffraction data taken from a sample that was synthesized at the University of Waterloo by Dr. Jamal Hassan can be found in his thesis[1].

CHAPTER 4

Water and Hydrogen Bonds

Introduction

Water is the most important substance to all organic life on Earth. All water on Earth is conserved and has a significant influence in the structural and physical properties of almost all living matter. Our understanding of water has been advanced significantly owing to theoretical and computational modelling[25]. Unfortunately different models address different aspects of water's behaviour. Simpler physical models that focus on more global properties of water such as solvation properties, thermodynamic properties, and phase behaviour will provide a better understanding of what we learn from the more complicated models. For example, the lack of a complete model which takes into account all of the underlying physics is responsible for our inability to predict protein structure or to design drugs. The design of fuel cells and 3-D MRI dosimeters, as well as ground water remediation are other areas of industry that would benefit from a complete model of water. Water has attracted the attention of both theoreticians and experimentalists. Useful

information regarding the structure and dynamics of water has been obtained from studies of dielectric relaxation, inelastic neutron scattering, and NMR nuclear spin relaxation and spectral approaches. Experimental NMR techniques allow for a variety of information concerning water structure and dynamics to be obtained. For example, the magnetic shielding of hydrogen or oxygen nuclei provides information about the average environment experienced by these nuclei in individual water molecules. Relaxation parameters for these nuclei can provide details about water molecule dynamics.

4.1 The Water Molecule

The water molecule is composed of two hydrogen atoms connected via covelent bonds to one oxygen atom as shown in Figure 4.1. The water molecule is sp^3 hybridized, with the oxygen atom centered on its 1s orbital accompanied by the hydrogen atoms occupying two of the four p orbitals[1]. The angle of the H-O-H bond is 104^o, and the O-H bond lengths are 0.97 Å. The O-H bond energy is 492 kJ mol^{-1}. The oxygen atom in each water molecule has two unshared pairs of electrons that can readily form hydrogen bonds with nearby hydrogen atoms.

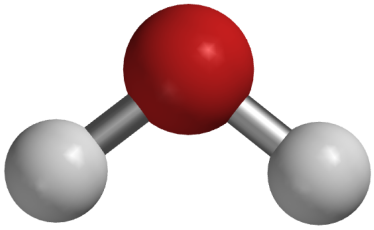

Fig 4.1: The water molecule. The oxygen atom is coloured red and the two hydrogen atoms are shown in white.

A widely accepted model of bulk water is a tetrahedral model where at room temperature the number of hydrogen bonds that each water molecule is involved in is about 3.6. This is very close to the value from the tetrahedral structure of Ice (I) which is 4. This enforces the condition that if a water molecule reorients or displaces itself, then most of the time it will be hydrogen bonded to one or more neighbouring water molecules[26]. Water molecule dynamics can be discussed in terms of rotational and translational motions characterized through correlation times τ_c. This value is widely accepted to be on the order of $\sim 10^{-12}$ seconds for both motional modes in water at room temperature. However, it has been observed that aqueous solutions, containing paramagnetic ionic species, can have correlation times as long as milliseconds[26] which are connected with the life time of a water molecule in the solvation shell. Additionally it has also been discovered that water molecules confined in porous media such as controlled pore glasses[27] and MCM-41[28] have correlation times as long as $\sim 10^{-6}$ s. The self-diffusion coefficient *D* gives us insight into the nature of the random translational component associated with the

random thermal motion of the water molecules.

$$\langle R^2 \rangle = 6Dt \qquad 4.1$$

where $<R^2>$ represents the mean square displacement of the water molecule after some time *t*. At 25°C the self-diffusion coefficient of water is $D = 2.31 \times 10^{-5}$ cm^2s^{-1}.

4.2 Hydrogen Bonds

Hydrogen bonding occurs when a hydrogen atom covalently bonded to an electronegative atom of one molecule (usually Oxygen , Nitrogen or Fluorine) is electrostatically attracted to another electronegative atom from a different molecule. The hydrogen bonding is a form of weak bonding that is generally stronger than the van der Waals interaction with a bond energy that depends on length and angle of the bond. The length of the hydrogen bond depends on temperature and pressure. Typical values for hydrogen bond energies range from 5 to 30 kJ mol^{-1}. In bulk water the length of the hydrogen bond H---OH is about 2.8 Å with a bond energy of about 17.5 kJ mol^{-1}. Figure 4.1 shows two water molecules which are hydrogen bonded together. This configuration is commonly referred to as the water dimer.

The underlying physical nature of the hydrogen bond is still debated by supporters of the electrostatic view, and others who support the idea that the hydrogen bond is 90%

ionic and about 10% covalent. Recently due to significant advances in computational power researchers have been able to employ ab-initio quantum chemical calculations in order to gain insight into the quantum mechanical nature of hydrogen bonding. This includes accounting for effects like tunneling, delocalization, and zero-point motion. Collectively in the literature these effects are commonly referred to as *nuclear quantum effects* and their treatment is beyond the scope of this thesis and the reader is referred to the relevant literature [29][30].

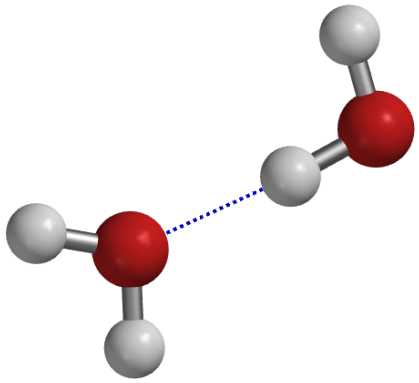

Fig 4.2: Hydrogen bonding between two water molecules shown as a dashed blue line. This configuration is commonly referred to as the dimer.

4.3 Silica-Water Systems

Since we are ultimately concerned with the behaviour of water at fractional surface coverages in MCM-41 it is appropriate to provide some details pertaining to the silica-

water interface. From an experimental point of view NMR, dielectric relaxation, and IR spectroscopy are thought to be the most powerful tools to investigate surface dynamics of water molecules confined in different silica materials.

The hydrated silica surface contains hydroxyl groups, also known as silanol groups, that present a very suitable surface for hydrogen bonding with water. Accordingly hydrogen bonding plays a central role in governing the dynamical properties of water molecules in these materials. Figure 4.3 shows a cristobalite fragment which hosts single silanol hydroxyl groups. Randomly intersecting cristobalite fragments have been proposed as a model for the MCM-41 surface (See section 7.1.1). Different hydration sites may exist on different silica surfaces due to

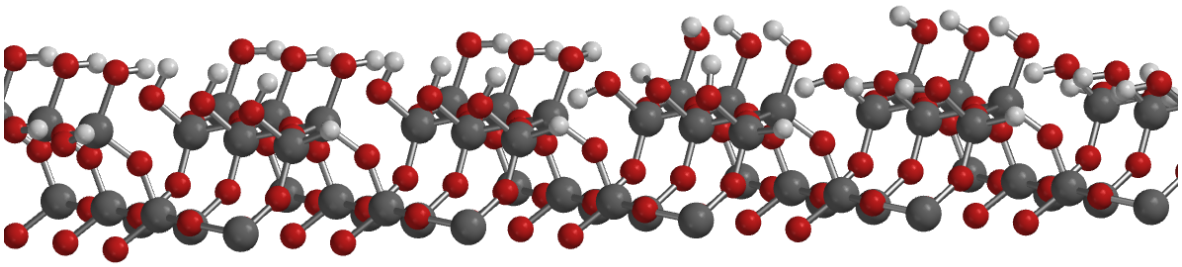

Fig 4.3: A slab of cristobalite which contains single silanol hydroxyl groups. Silicon atoms are shown in grey, oxygen atoms are in red and hydrogen atoms are coloured white. Each silanol group presents three hydrogen bonding sites; two on the oxygen atom and one on the hydrogen atom.

the various geometrical arrangements of the silanol groups that may be encountered. A

study of the quartz water interface revealed the presence of two types of surface water which were each attributed to different hydration sites in the material[31]. NMR studies of hydrated controlled pore glasses[25] have shown that water adsorbed to the surface exhibits slow components (~10^{-6} s) in its motion. Water molecules in MCM-41 also exhibit decreased mobility[28][32] with translational diffusion times which are slower than for bulk water. However, an accurate diffusion model with well defined diffusion coefficients in hydrated MCM-41 is not available. It has also been observed that water has a depressed freezing point when confined in pores of various silica nanostructures. For example during this study, at low hydrations, no freezing of the pore water was observed at all (discussed in more detail in Chapter 6).

Various NMR studies performed on samples containing water in porous silica systems have interpreted the results based on magnetization exchange models. One study[33] using deuterium oxide (D_2O) interpreted the results based on a three site magnetization exchange model in which two exchange rates of 1000 s^{-1} and 300 s^{-1} between water groups is reported. Another study[34] of partially hydrated MCM-41, using ^1H MAS NMR, concluded that water hydrogen bonded to surface silanol groups is understood to be under conditions of fast exchange at rate of about 10 ms^{-1}. These studies simply refer to magnetization exchange and do not mention whether chemical exchange, magnetic exchange or physical exchange is the dominant process. Another prominent research group[2] has proposed that the ^1H MAS NMR spectrum of hydrated MCM-41 can be interpreted in terms of a fast chemical exchange model in which hydrogen bonded protons are exchanging with one another or in terms of a surface hopping model. It has been

recently shown[3] that the concept of magnetization exchange of any kind is not needed to explain the observed NMR spectra.

In this study a model for the spectral behaviour of hydrated MCM-41 with temperature and hydration was developed which does not involve magnetization exchange. The NMR results instead are interpreted based on the self-diffusion of water molecules along the pore surface of MCM-41. The model is presented in detail in Chapter 6.

CHAPTER 5

Experimental Section

5.1 Sample Preparation

The description concerning the preparation of the hydrated mesoporous MCM-41 samples will be provided in this section. The MCM-41 material was obtained from Sigma-Aldrich chemical company in its unhydroxylated form. Thus the primary step towards obtaining the NMR samples involves hydroxylating the silica surface to create the surface silanol groups. This essentially involves the reverse of the dehydroxylation reactions shown in Figure 3.1. To achieve this, MCM-41 was packed into the uncapped zirconia MAS rotor and placed into a glass test tube. The test tube was filled with enough distilled deionized water (UW Chem Stores) to completely submerge the rotor and attached to a vacuum system. The samples were then pumped on while maintaining a slow, controlled decrease of pressure, until tiny bubbles could be seen leaving the rotor. The sample was then closed to the vacuum until the bubbles subsided. This process was repeated 4-5 times to ensure that water has completely filled the pores and thus the optimal hydroxylation conditions had

been reached. The submerged rotor containing the MCM-41 was left under vacuum for 48 hours to ensure complete hydroxylation of the surface had taken place. Using a pasteur pipette, the bulk water in the test tube was removed leaving the water soaked MAS rotor and MCM-41 behind. The excess water saturating the rotor was removed by reattaching the sample to the vacuum system and pumping for 30 hours with the sample at 80 ^{o}C to ensure that only hydrogen bonded and single silanols groups remain. To make sure that no water from the air could contaminate the sample during placement of the cap on the rotor, the sample was transferred under vacuum to a glove box which contained a dry nitrogen atmosphere . After capping the sample a weight measurement was taken using a Pinnacle Series PI-225D micro balance which provided an accuracy of $\pm 1 \mu g$. The final weight of the dry hydroxylated MCM-41 and the capped MAS rotor was measured to be 0.69176 grams.

This study involves investigating water dynamics at fractional monolayer coverages; specifically coverages up to 0.2 monolayers. The specific surface area of the MCM-41 obtained from Aldrich was determined using nitrogen adsorption measurements (see Appendix I). The available surface area was found to be ~1132 m^2/g and if one assumes water molecules of dimensions 3x3 Angstroms (van der Waals radius for a water molecule is 1.7 Å) occupying a square lattice then one finds that for 1 gram of MCM-41 0.34 grams of water are required to completely cover the surface or to form a monolayer. To hydrate the samples the rotor was uncapped and placed in a desiccator containing water vapor. Vapor phase hydration was allowed to proceed for a fixed amount of time after which the rotor was capped and weighed to determine how much water had been introduced into the

sample. The various times spent in the desiccator and resulting hydration levels are tabulated and shown in Table 5.1. NMR experiments were performed for each hydration level over a temperature range of 200 K-325 K.

Desiccator Time (min)	Sample Weight (g)	Water Weight (g)	Hydration Level (% by weight)	Hydration Level (monolayers)
0	0.69176	0	0	0
10	0.69210	0	0.9%	0.027
20	0.69227	0.00051	1.3%	0.038
35	0.69265	0.00089	2.3%	0.070
50	0.69296	0.00120	3.0%	0.091
70	0.69370	0.00194	4.9%	0.148
90	0.69411	0.00235	6.0%	0.182
110	0.69437	0.00261	6.6%	0.194
150	0.69485	0.00309	7.8%	0.229

Table 5.1: Gravimetric measurements of the hydrated MCM-41 sample.

5.2 Fourier Transform NMR

In Chapter 2 the concept of the free induction decay or FID was introduced. The oscillating magnetization vector consists of the vector sum of all the responses from all the spins which have been excited via RF pulses. Due to properties of the Fourier transform, such pulses excite the nuclear spins resonating within a certain bandwidth that is

inversely proportional to the pulse length since an electronic square wave is essentially made of many oscillating sinusoidal components, each at a frequency in the“neighbourhood”of the carrier frequency. To acquire the frequency domain NMR spectrum one must therefore Fourier transform the time domain FID. Coincidentally the development of Fourier Transform NMR and the development of digital computers and the Fast Fourier Transform (FFT) occurred simultaneously. Most commercial systems today implement a FFT algorithm in order to acquire the frequency domain spectrum. Richard Ernst is considered the pioneer of FT-NMR and in 1991 won the Nobel Prize for achievements in this field.

If the time domain signal decays exponentially the FT of the time domain signal is a Lorentzian function in the frequency domain. The expression for a Lorentzian line-shape is of the form

$$y(\nu) = y_o + \frac{2A}{\pi}\left(\frac{w}{4(\nu-\nu_c)^2 + w^2}\right) \qquad 5.1$$

A is the area under the line and is proportional to the number of spins in that environment. The parameter *w* represents the full-width at half-maximum (FWHM) of the line, and ν_c is the center frequency which is usually defined in ppm. All the data in this work are analyzed and interpreted based on fitting the results to Lorentzian lineshapes.

5.3 Magic Angle Spinning (MAS)

In most solid state experiments, the nuclei in the condensed phase experience strong interactions (dipolar, quadrupolar) which quite often lead to very broad and featureless spectra. These interactions, in solids, can be averaged out by spinning the sample at the so called *magic angle,* $\theta_M = 54.74^o$. This comes about as follows. Under fast, mechanical rotation of the sample about an axis that makes an angle θ_M with $\vec{B}_o$ the $(1-3\cos^2\theta)$ term which appears in the dipolar Hamiltonian should be replaced by its average value which can be written as[35].

$$\overline{(1-3\cos^2\theta)} = (1-3\cos^2\theta_M)\frac{3\cos^2\phi - 1}{2} \qquad 5.2$$

The angle ϕ represents the angle formed between the internuclear vector and the axis of rotation. For fast rotation at $\theta_M = 54.74^o$, the first term appearing on right hand side of equation 5.2 goes to zero, effectively removing the effect of dipolar couplings. The result is a spectrum with increased resolution providing the isotropic chemical shift values, which are of interest for structural determination of the solid state.

The samples for the MAS experiments were packed into 4mm diameter zirconia rotors (Bruker) and then capped with zirconia rotor caps supplied by Wilmad LabGlass Company. A 4 mm 15 kHz Bruker MAS probe was used for all the experiments which involved spinning of the sample. The physical spinning of the sample was achieved by

blowing dry N_2 gas through the fan-shaped rotor cap. The spinning rate was set to 10 kHz and was controlled using a Bruker MAS Pneumatik Control Unit. A Bruker BVT3000 temperature controller maintained the sample temperature at the desired value.

5.4 NMR Apparatus

Besides the magnet, the hardware associated with NMR is much akin to that of radio or radar transmission/reception in which electronics are required to switch between transmit and receive modes. In pulsed NMR the power levels associated with the pulses are on the order of kilowatts whereas the signals coming from the sample are on the order of picowatts. As such, at the heart of every NMR spectrometer is an RF transceiver. The overall block diagram of a typical high resolution pulsed NMR spectrometer is shown in Figure 5.1.

All spectra were obtained using a 11.7 Tesla Bruker superconducting magnet with a bore size of 89 mm. A Bruker DMX500 spectrometer running XWINNMR software on a Unix based workstation was used to acquire and Fourier transform the data. The frequency domain data were then exported for analysis in the Origin software environment.

5.5 ^{1}H MAS NMR Measurements

Sixty-three single $\pi/2$ pulse ^{1}H NMR MAS experiments were performed covering an array of seven different temperatures and nine different hydration levels. Specifically experiments were performed at temperatures of T=200 K, 225 K, 250 K, 270 K, 293 K, and 325 K. The hydration levels covered are listed in Table 5.1 which can be found in the section 5.1. The resulting FIDs were Fourier transformed into the frequency domain and exported for peak analysis. The chemical shift calibration was done using a DSS sample.

The pulse excitation length was set to 3.80 μs with a repetition time of 6 s. A total of 64 accumulations per spectrum were acquired to ensure proper averaging of the signal. A minimum of 4 accumulations is required for quadrature detection. The repetition time was set to 1 s to ensure the magnetization had returned to its initial M_o value prior to the next pulse.

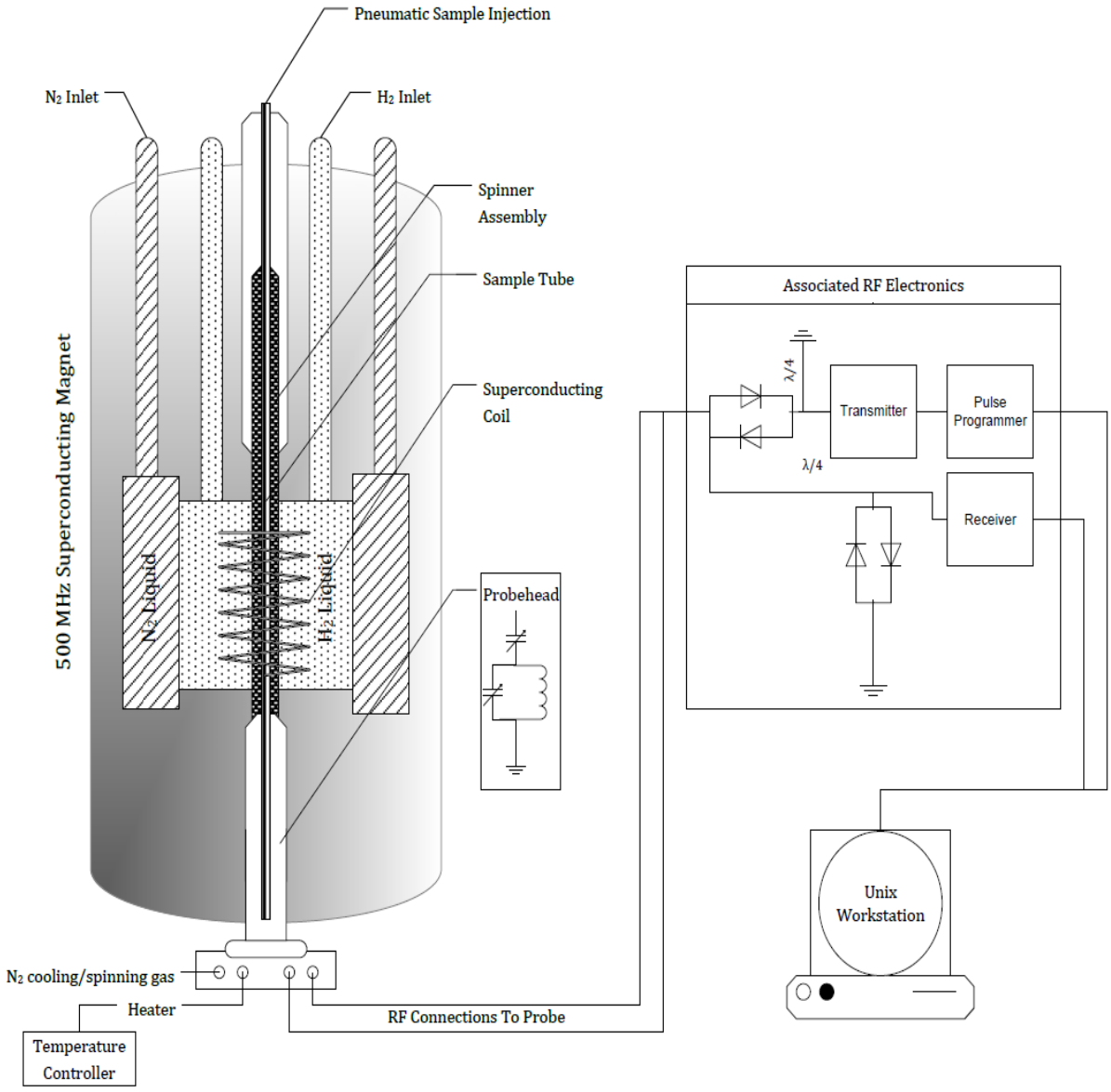

Fig 5.1: Typical high-resolution NMR spectrometer shown with associated radio-frequency electronics components. Two sets of cross diodes and a pair of transmission lines provide electrical isolation of the transmitter and receiver. PIN diodes can also be used which provide even better isolation and switching characteristics.

CHAPTER 6

Results, Model, Discussions

6.1 ^{1}H NMR Results

Proton NMR experiments using MAS (described in previous chapter) were performed on samples with 0 to 7.8% hydration by weight and over the temperature range of 200 to 325 Kelvin. The spectra for the unhydrated samples are displayed in Figure 6.1 for all temperatures. The results for T=200 K, 250 K, and 300 K are shown in Figure 6.2 for hydration levels of 2.3%, 4.9%, and 7.8%. The significance of studying roughly up to ~7-8% hydration by weight is that the ratio of water molecules to surface silanol groups approaches 1:1. The remaining spectra can be found in the Appendix I.

In terms of what is detected by the proton NMR experiment, the samples are composed of water protons and the various Q silanol protons involved in the different isolated and hydrogen bonded configurations. It is believed that[2][34] magnetization exchange processes between OH surface protons and water protons play an important role

in producing the spectral lineshapes which are seen in Figure 6.2.

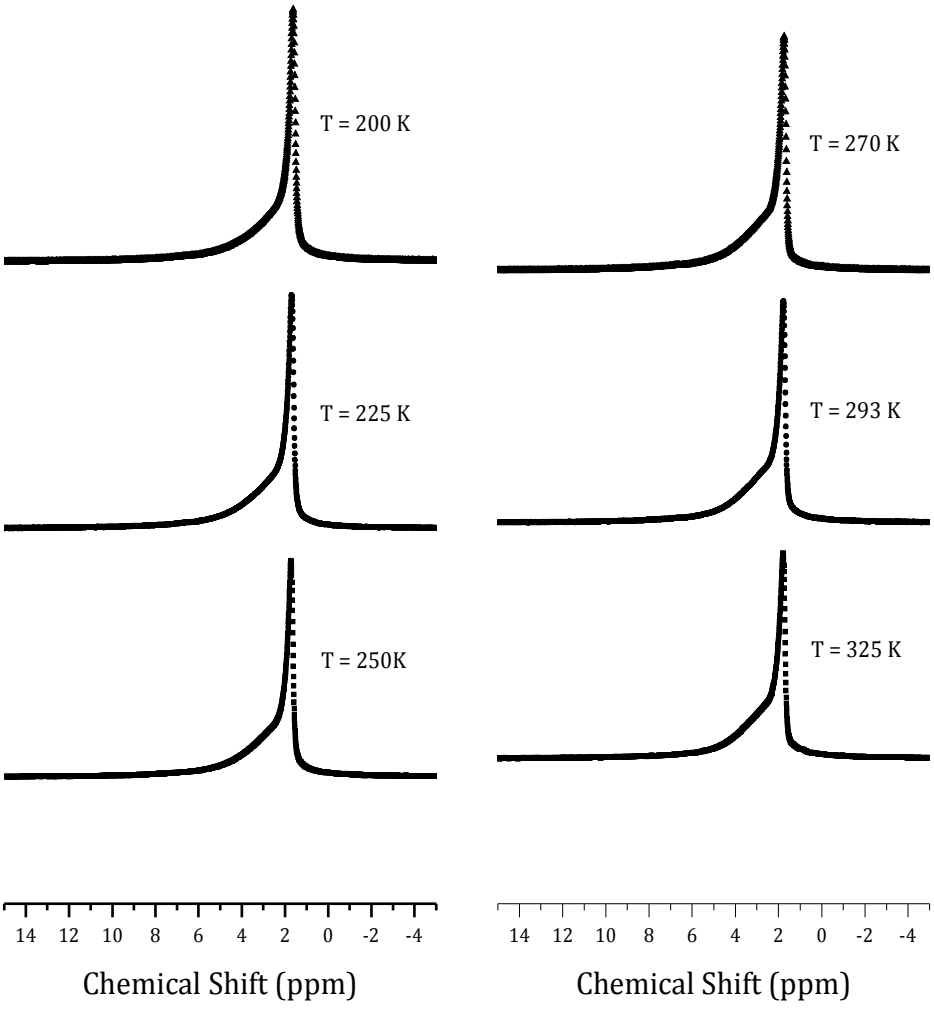

Fig 6.1: ^{1}H MAS NMR spectra for dry (unhydrated) MCM-41 shown at all temperatures studied.

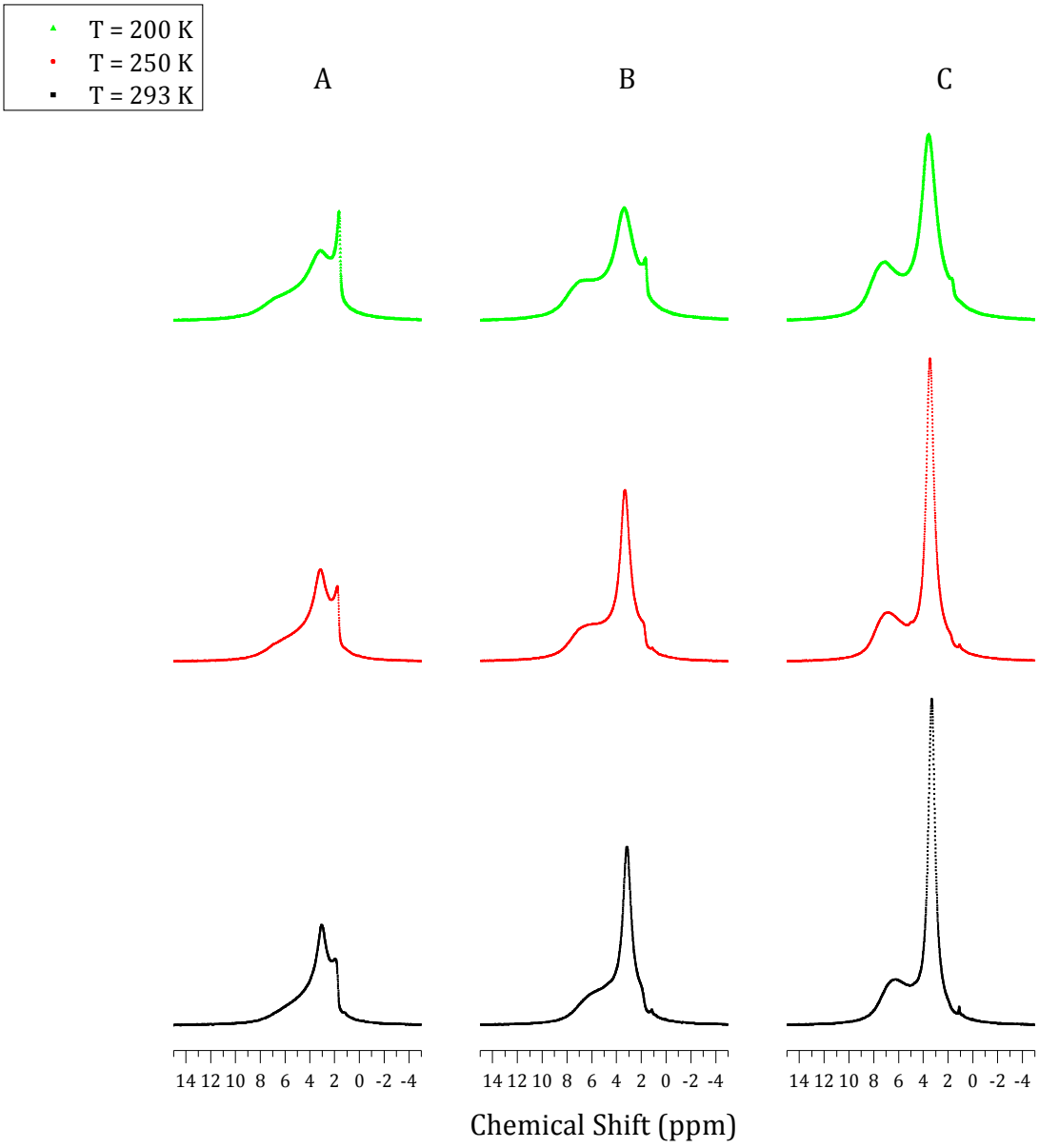

Fig 6.2: ^{1}H MAS spectra for hydrated MCM-41. Raw, experimental data (no temperature correction) is shown for three of the hydration levels studied (see Appendix I for remaining data). Spectra for hydrations of 2.3%, 4.9%, and 7.8% by weight and are shown in columns A, B, and C, respectively.

6.2 Model for chemical shift averaging

A simplified model based on chemical shift averaging ($\delta_{\text{H-bonded}}$ and $\delta_{\text{not H-bonded}}$) due to rotational and translational motion of water on the pore surface has been developed in order to predict the chemical shifts and resonance peak areas for each spin group involved. The model is able to reproduce the experimental ^{1}H MAS NMR data for all hydrations and temperatures studied. Surface OH group proton-water proton magnetization exchange is not needed to explain the present results.

6.2.1 MCM-41 β-Cristobalite Surface Model

As discussed in chapter 3, the MCM-41 surface has both single and hydrogen bonded silanols. To establish a basis for the present model we must first consider all the possible hydrogen bonding configurations that can exist between water molecules and the amorphous silica surface, which contains the silanols groups. A widely accepted model for the silica surface based on random intersecting segments of (111) and (100) β-cristobalite crystalline surfaces[36] was used to establish the possible geometric configuration of the surface hydroxyl groups and consequently the coordination of water molecules (see Figure 6.3).

In this surface model the single silanols are situated on the (100)-type face and the

geminal silanols can be found on the (111)-type faces of β-cristobalite crystallites. The average distance between the hydroxyl groups on the (100)-type faces is roughly 0.5nm and is too far for any of them to form hydrogen bonds with each other [36]. The geminal groups however can have their hydroxyl groups form hydrogen bonds depending on their relative orientations. In addition, in keeping with the literature, it is considered that hydrogen bonding in MCM-41 also occurs at convex type intersections of these crystallites.

6.2.2 Water Coordination and Associated Chemical Shifts

In the proposed model each water molecule is limited to making at most two hydrogen bonds to the model surface at any given time. A water molecule forming three (or more) hydrogen bonds to three separate surface silanol groups is considered a highly specialized configuration and is thought to exist in very low numbers in the temperature range studied. The various conformations of water molecules on the MCM-41 surface, considered in this study, are shown in Figure 6.3 and are labelled a-g. Also shown are the associated chemical shifts (at room temperature) of silanol and water protons in each configuration. These conformations in themselves are not new and have been previously presented by the other research groups[3][34] as possible conformations that one might find when investigating the hydrated silica surface. The chemical shifts were calculated using ab-initio quantum chemistry recipes as described in section 2.3. In addition, it is proposed that since the model addresses hydration levels at fractional monolayer coverages (up to

~0.2 monolayers or ~20 % surface coverage) water-water interactions are negligible.

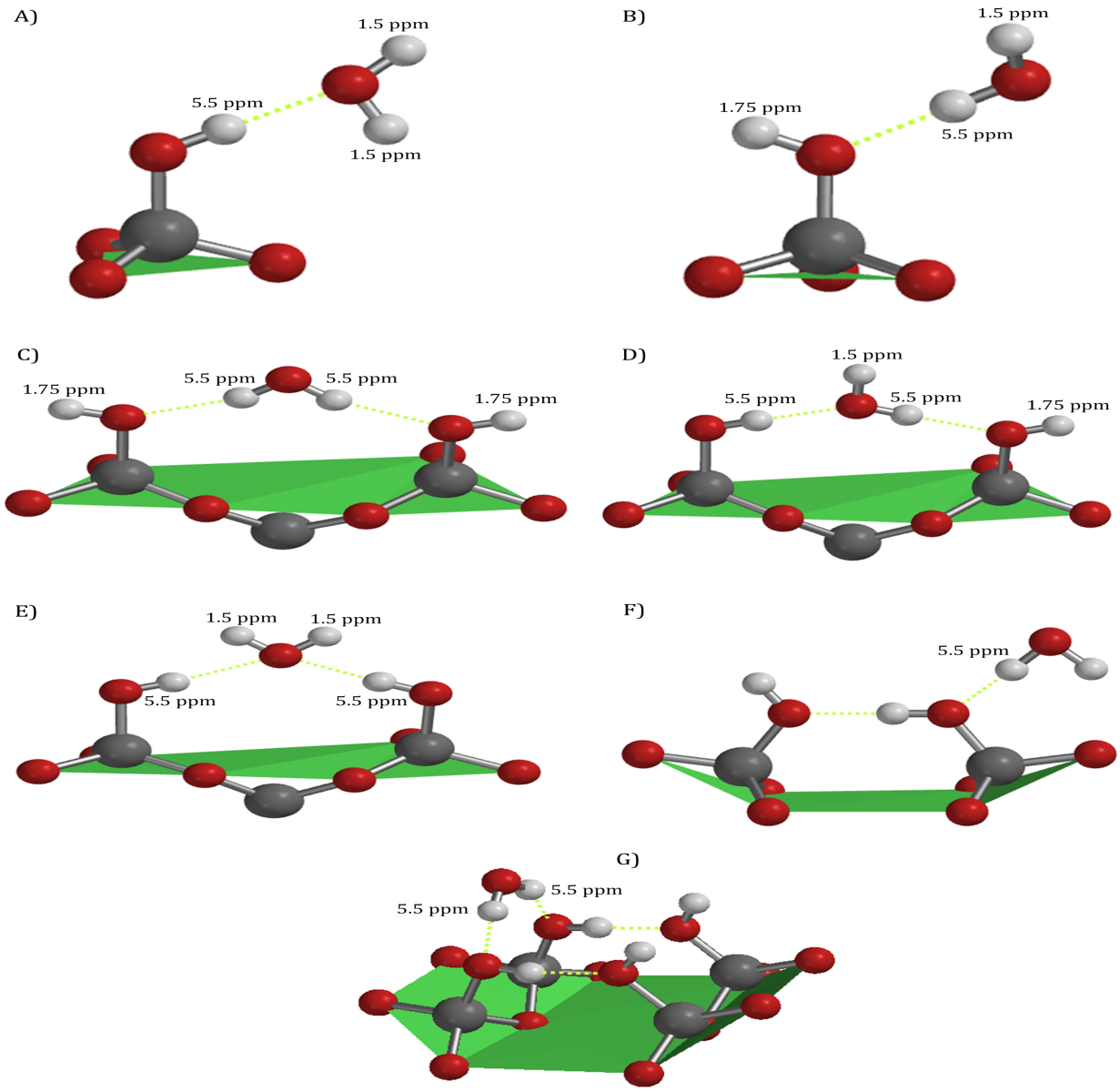

Fig 6.3: The various hydrogen bonding conformations, A-G, to the surface silanols considered in the chemical shift averaging model . Dotted green lines represent hydrogen bonds. All protons involved in hydrogen bonding are assumed to take on the same isotropic chemical shift value[33]. Calculated shifts are for T ~ 293 K.

Water coordination to hydrogen bonded hydroxyl groups has not been previously reported on and in the present model it is assumed that hydration to the hydrogen bonded groups occurs only via water hydrating the oxygen of the hydrogen bonded hydroxyl groups. As a first approximation this will leave the chemical shift of the surface protons unaltered for these cases. The basis for such an assumption is that all hydrogens in the hydrogen bonded silanol groups, forming a hydrogen bond, are involved in hydrogen bonding to their maximum capacity and within the oxygen atom one or two orbitals remain for water to form a hydrogen bond, should the opportunity arise.

6.2.3 Effect of rotational motion and self-diffusion of water molecules on the apparent populations of each spin group.

In order to model surface coverage for hydrated MCM-41, at fractional monolayer coverages, using a self-diffusion scenario, we first assume that the average water molecule adsorbed onto the surface of MCM-41 remains on the surface. In addition, it is assumed that the water molecules diffuse on the surface in a completely random fashion without preference for single or hydrogen bonded OH groups. Then 62% of the water molecules are expected to hydrate the hydrogen bonded OH groups and 38% are hydrogen bonded to single silanols in the various conformations shown earlier. This comes about from the dry spectrum (Figure 6.1) of MCM-41 where it was found that the ratio of hydrogen bonded

silanols to single silanols is approximately 3:2.

As the water molecules diffuse on the surface they visit hydration sites making hydrogen bonds in different conformations resulting in a deshielding of the various protons involved (See figure 6.3). If the thermal energy available to the water molecule is high enough it is expected that a single water molecule can hydrate or visit multiple (more than one) hydroxyl groups over the NMR experimental timescale (~1 ms). In addition it is assumed that as the hydration level is increased at constant temperature, the number of hydrated or visited silanol species is linearly proportional to the number of water molecules present on the surface through a "visiting parameter" *J*:

$$\#OH_{hydrated} \approx J\left(N_{water}\right) \qquad 6.1$$

J is related to the number of translational jumps, or steps, a water molecule takes during the experimental timescale. The jump parameter is expected to depend on the two-dimensional diffusion constant for water on the surface and temperature. The jump parameter ultimately defines the areas present under the hydrated and unhydrated single hydroxyl peaks. Since the hydrogen bonding of water molecules to hydrogen bonded silanols is proposed to only occur via the oxygen atoms of the hydroxyl groups, the area for this peak would remain unchanged from the dry spectrum since these hydroxyl protons experience no shift due to hydrogen bonding with water molecules.

The total water peak area, which represents hydration water, is directly proportional to the number of water molecules present on the surface. However there are

two subgroups, and thus two sub-areas of water signals which make up the total water resonance area: water molecules involved in hydrogen bonding to single silanols and water molecules involved in hydrogen bonding to hydrogen bonded silanols. Therefore, in keeping with the model, 62% of the water area is assigned to water interacting with hydrogen bonded OH groups, and the remaining 38% to water interacting with the single silanols groups. The fractions for these two water groups is assumed to be constant.

6.2.4 Effect of water molecule surface dynamics on the observed chemical shifts

Six spin groups have been identified for partially hydrated (≤ 0.2 monolayer) samples of MCM-41 in this discussion: two unhydrated silanol groups, two hydrated silanol groups, and two water groups. In order to ascertain the possible chemical shifts of spin group we follow an approach which will make as few assumptions as possible in terms of hydration details and conformations. As a first approximation we assume, that since even at low hydrations the thermal energy is high enough and the water molecule motion is fast enough for a molecule of a particular group to sample all conformations for that group in the experimental timescale. Then one must observe an average chemical shift for each spin group, based on averaging the chemical shifts of the protons for all conformations available to that particular group, weighted by the probability of the conformations. In essence this is implying that the jump parameter described in the

previous section should take on values which indicate that a water molecule is able to visit multiple hydrations sites over the experimental timescale.

Following the procedure outlined above the possible chemical shifts for each of the 6 spin groups will be deduced. Let us start with the simplest case, the unhydrated single and hydrogen bonded silanols. The chemical shifts for these spin groups is well established[1][2][28] and are usually taken to be $\delta_{S\text{-}OH} = 1.75$ ppm and $\delta_{HB\text{-}OH} = 2.6$ ppm in dry MCM-41. However, as the hydration level is increased the chemical shift distribution, and their centers, which define these spin groups will change. This comes about due to changes in the average environment experienced by the surface hydroxyl groups as neighbouring silanol groups have to reorient themselves in order to accommodate a favourable hydrogen bonding coordination with the water molecules being added[37]. Such influence by neighbouring silanol groups will also vary with temperature. Here $\delta_{S\text{-}OH}$ and $\delta_{HB\text{-}OH}$ will be allowed to vary during the fitting process.

Since we have restricted the hydrogen bonding details concerning the hydrogen bonded groups to the two coordinations shown in Figure 6.3f and 6.3g, the details concerning the chemical shift of the hydrated hydrogen bonded groups become straight forward. The average chemical shift value for hydrogen bonded silanols is expected to vary only slightly due to changes in the environment resulting from a change in temperature or hydration causing a reorientation of the neighbouring surface silanols.

The chemical shift details regarding the hydrated single silanol groups requires averaging over all the possible conformations that can occur for this group weighted by the probability for each coordination to occur. Therefore the chemical shift at room

temperature for this spin group is given by,

$$\delta_{OH_{hydrated}} = p_A(1.75) + p_B(5.5) + p_C(5.5+1.75) + p_D(1.75+1.75) + p_E(5.5+5.5 \qquad 6.2$$

where p_A, p_B, p_C, p_D and p_E represent the fractional probability of each coordination occurring. The subscripts refer to the conformations appearing in Figure 6.3. For example if all conformations are thought to be equally likely, then according to the above formalism the chemical shift for the hydrated single silanol group would equal 3.625 ppm.

The proton chemical shift of each water molecule in a given conformation is the average chemical shift of the shifts of the two protons in the water molecule. The chemical shift associated with the water protons hydrating the single silanols depends on p_A, p_B, p_C, p_D and p_E as well and has the form

$$\delta_{Water_{S\text{-}OH}} = p_A(3.5) + p_B(1.5) + p_C(3.5) + p_D(5.5) + p_E(1.5) \qquad 6.3$$

If one assumes that all conformations are equally sampled then the hydration water associated with single silanols will have a chemical shift of about 3.1 ppm.

There are only two conformations that water molecules, which hydrate the hydrogen bonded groups, can assume (Figure 6.3 f and g). These involve the water molecule to either have one of its hydrogens hydrogen bond to one oxygen of a hydrogen bonded hydroxyl group, or to have both of its hydrogens hydrogen bond to two different oxygens from two hydrogen bonded OH groups. The chemical shift of this water group is

$$\delta_{Water_{\text{HB-OH}}} = p_F\left(\frac{5.5+5.5}{2}\right)+p_G\left(\frac{5.5+1.5}{2}\right) \qquad 6.4$$

Taking both conformations to be equally probable results in a chemical shift of 4.5 ppm.

The chemical shift values used in the calculations presented are for room temperature. Protons involved in hydrogen bonding are well known to have their chemical shifts vary linearly with temperature[38][39]. The data found in[39] can serve as a guide in determining the temperature dependance of the chemical shift of hydrogen bonded protons in hydrated MCM-41. Additionally experimental data can be used to determine the approximate value of the chemical shift of protons involved in hydrogen bonding at a certain temperature by identifying the center of the highest shifted visible peak in the spectrum of a hydrated sample. The center of this peak serves as indicator as to what the average chemical shift of a hydrogen bonded proton might be in this system without any averaging effects. To this end it is useful to consider the spectrum associated with the highest hydration level since this provides a clear definition of this peak. If we consider the spectra in Figure 6.2 for the hydration level of 7.8% by weight, it is seen that there is indeed a connection between this peak center and temperature. At 325 K we see that the center of the highest shifted peak is at around 5.5 ppm, whereas at 200 K it is around 7 ppm . Thus in the chemical shift calculations above, one would simply change the shifted values of 5.5 ppm to 7.1 ppm and then proceed to calculate the average chemical shift for each spin group based on the imposed weighting as one sees fit. The preceding discussion serves to indicate how we can model the chemical shift as a function of temperature. In this

study these parameters will be varied when fitting the data. Linear behaviour is expected with changing temperature which will confirm these ideas.

The idea of equally weighting the populations of each conformation was only for illustrative purposes. In general it is unknown what the populations p_N of each conformation might be. Thus the average chemical shift for each spin group is allowed to vary during the fitting process. Since the model can only predict the average chemical shift for the two water groups as well as for the hydrated and unhydrated surface hydroxyl groups, obtaining the values of p_N becomes non-trivial.

The calculated average chemical shift for each spin group serves as an indicator as to whether or not water is forming one or two hydrogen bonds on average. If one considers equations 6.2, 6.3, and 6.4, then it becomes clear that the centers of the lines are inter-dependant based on the populations p_N. For example, an increase in the isotropic chemical shift value for the water group hydrating the single silanols groups is indicative of more and more water molecules forming hydrogen bonds to the oxygen atoms of the MCM-41 surface. Correspondingly one should then observe a decrease in the chemical shift value defining the hydrated single silanols. Furthermore, increases in chemical shift values for the water protons can be interpreted as an increase in the number of water molecules forming two hydrogen bonds to two separate silanol groups, as diagrammed in Figure 6.3g. This is the only conformation that can drive the chemical shift value for the water groups to its maximum value at a given temperature.

6.2.5 Effect of water molecule surface dynamics on the observed chemical shift distribution

For a completely unhydrated sample of MCM-41 the linewidths associated with the single and hydrogen bonded silanols under conditions of MAS has been found to vary only slightly over the range of temperatures studied (see Figure 6.1). Recall, however, that as water is introduced into the pores of the material where it begins to visit hydration sites, the chemical shift distributions for both the hydrated and unhydrated silanols will change as discussed in the previous section. Thus, the linewidths associated with all of the spin groups will be allowed to vary during the fitting process with the following guidelines. First, the linewidth for the unhydrated single silanols will be allowed to vary only slightly and likewise for both the unhydrated and hydrated hydrogen bonded silanol groups. Second, the model proposes that cristobalite surface segments, which contain the single silanol groups, present more hydrogen bonding conformations for adsorbed water molecules than for the hydrogen bonded silanols (only two conformations allowed). Following this line of thinking one would expect the chemical shift distribution, and hence the linewidth for water hydrating the single hydroxyl groups, to be broader than that associated with water adsorbed onto hydrogen bonded hydroxyl groups. However, the populations p_N also play a role in establishing the linewidth. For example, if there exists only one conformation for water molecules involved in hydrogen bonding to the surface silanols groups of MCM-41 then one would observe a relatively narrow line. If many

different conformations (environments) are likely to be found then one would observe a relatively broader line. In addition, it is not known a priori how the linewidth of the single silanol species have their associated linewidth change with temperature. Consequently the parameter associated with this value will be allowed to vary during the fitting process. Assuming the linewidth is largely controlled by the distribution of chemical shifts then the linewidth ultimately depends on the number of different environments that the single silanols, which are hydrogen bonded to water, are experiencing. As discussed in the previous section, changes in the linewidth are interpreted as changes in number of coordinations involved and changes in their corresponding populations.

An example will follow to illustrate how to the proposed model can be used to simulate various NMR spectra. For this purpose consider a hydration level where the ratio of the number of water molecules to surface hydroxyl groups is 1:1. Then on average all of the single OH peak, which is centered at 1.75 ppm, has now been completely shifted. As discussed earlier the ratio of hydrogen bonded groups to single OH groups is roughly 3:2. Therefore at this hydration level 20.7% of the total area will represent the hydrogen bonded groups, 41% percent of the area will be due to the water hydrating the hydrogen bonded groups, 12.6% will represent the completely shifted single silanol group, and 25.3% will come from the water hydrating these single silanols.

If we take the temperature to be ~293 K, then the proton chemical shift of hydrogen bonded species is 5.5 ppm. Furthermore, an equal probability for each hydrogen bonding coordination discussed in the previous section will be imposed. Accordingly the chemical shifts for the hydrogen bonded silanols and the respective hydration water, and the shifted

single silanols plus their hydration waters are 2.6 ppm, 4.5 ppm, 3.6 ppm, and 3.1 ppm, respectively.

Up to this point modelling the linewidth has not been discussed. The single silanol peak and hydrogen bonded silanol peak, in their unhydrated forms, have well defined linewidths which can be injected into the model directly [1][3][28]. In addition, due to the restricted conformations of the hydrated hydrogen bonded silanols, the linewidth associated with these protons is assumed to remain unchanged. However, one does not know the specifics regarding how the linewidths associated with the hydrated single hydroxyl groups and the associated hydration water change with temperature or hydration.

The system of study essentially consists of hydrogen bonded oxygen and hydrogen atoms. Accordingly, the linewidth associated with the hydrogen bonded hydroxyl groups is expected to provide a good estimation of the linewidth for single silanols which have become hydrogen bonded to the oxygen of a given a water molecule. Therefore the linewidth associated with the hydrated single silanol peak can be taken to be identical to that of the hydrogen bonded silanols.

6.2.6 Initial application of the chemical shift averaging model to spectra in hydrated MCM-41

The chemical shift averaging model with the above restrictions (section 6.2) was used to initially fit the data (with 7 adjustable parameters). The 7 adjustable parameters

are;

- the centers of the unhydrated/hydrated single silanol group
- the linewidth of the hydrated single silanol group
- the centers of the two water groups
- the linewidths of the two water groups

Representative fits are shown in Figure 6.4. The remaining spectra are shown in Appendix II. Figure 6.5 gives the plots of the spectral parameters obtained for all hydration levels and temperatures of 200 K, 250 K, and 293 K. Figure 6.6 gives the plots of the spectral parameters obtained for all temperatures and hydration levels of 2.3 %, 4.9 %, and 7.8 %. Relative little scatter is seen in the parameters with temperature and hydration. Correspondence between experimental and modelled/fitted spectra (Figure 6.4) is clear. This is taken to indicate that the 5-peak model provides a reasonable prediction of the data. The quality of the fit is expected to improve by increasing the number of adjustable parameters.

In the previous sections (section 6.2) the chemical shift averaging model was discussed in detail in which 5 peaks are defined. It was proposed that these peaks will be fit to the data with only four of the parameters defined; specifically the area of the hydrogen bonded silanol peak, the area of the hydrated single silanol peak, and the areas of the water groups. This leaves 11 parameters which could be varied during the fitting process. Using 11 adjustable parameters may be seen as over-fitting the data. However, it was felt that as long as limited significance of the temperature and hydration dependance of parameters is expected, and any trends observed are physically expected or reasonable,

the improved match between model and experiment is desirable. Such a fitting process is applied in the next section.

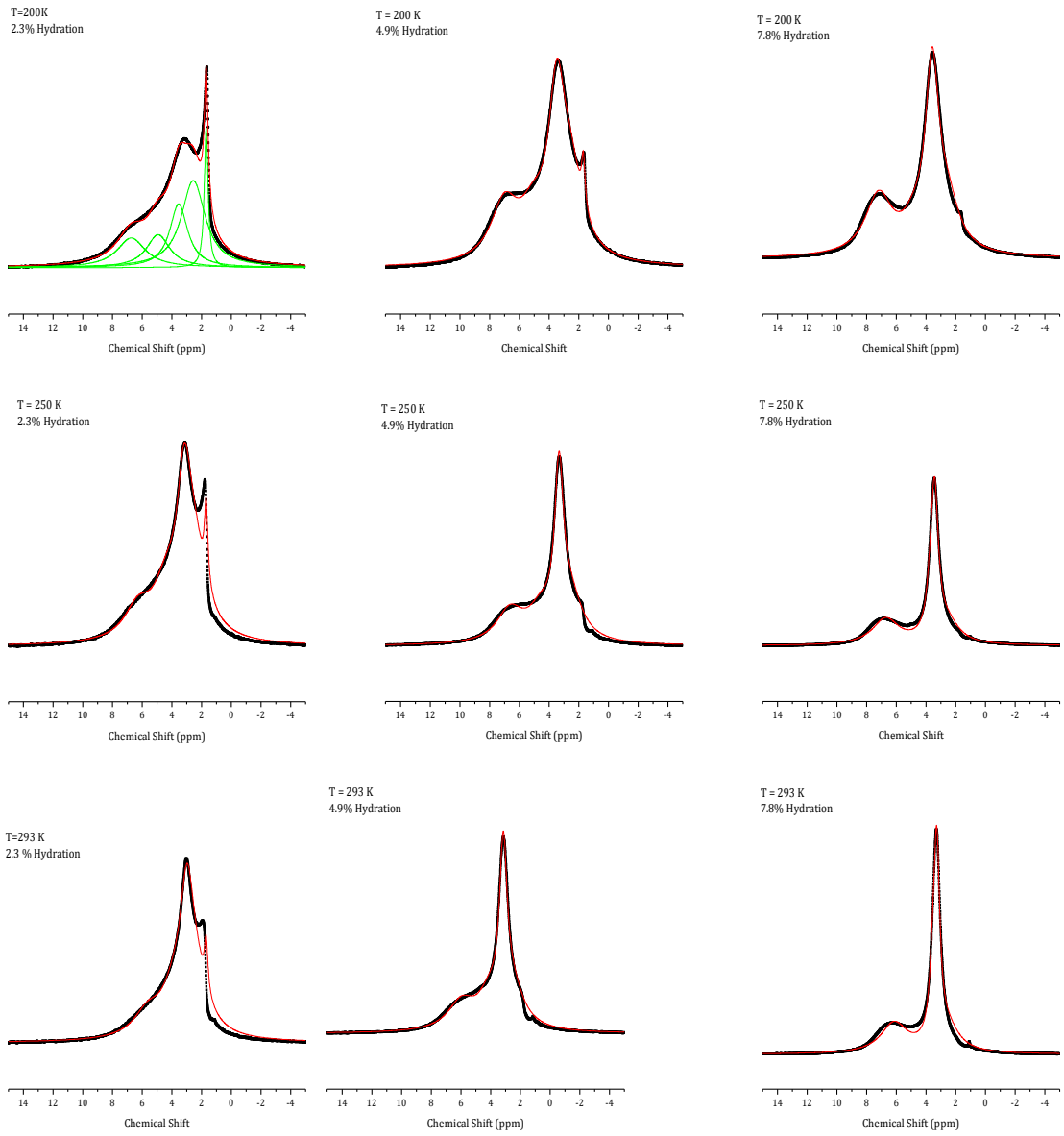

Fig 6.4: ^{1}H MAS NMR spectra of hydrated MCM-41. Spectra fitted (red line) using the model in which 7 parameters were allowed to vary in order to ascertain the whether or not the 5-peak model provides a reasonable prediction of the data.

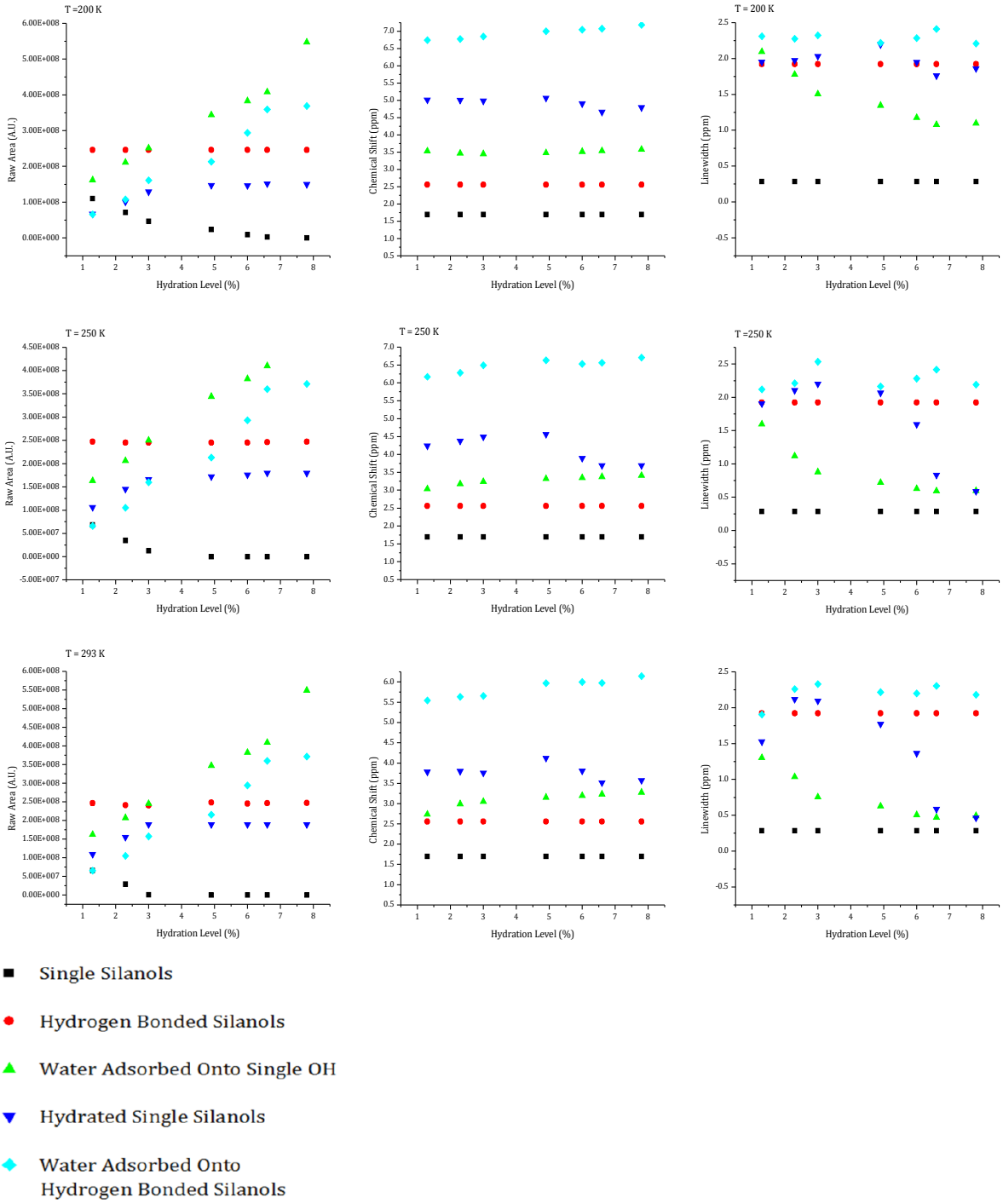

Fig 6.5: Hydration dependance of the fitted parameters.

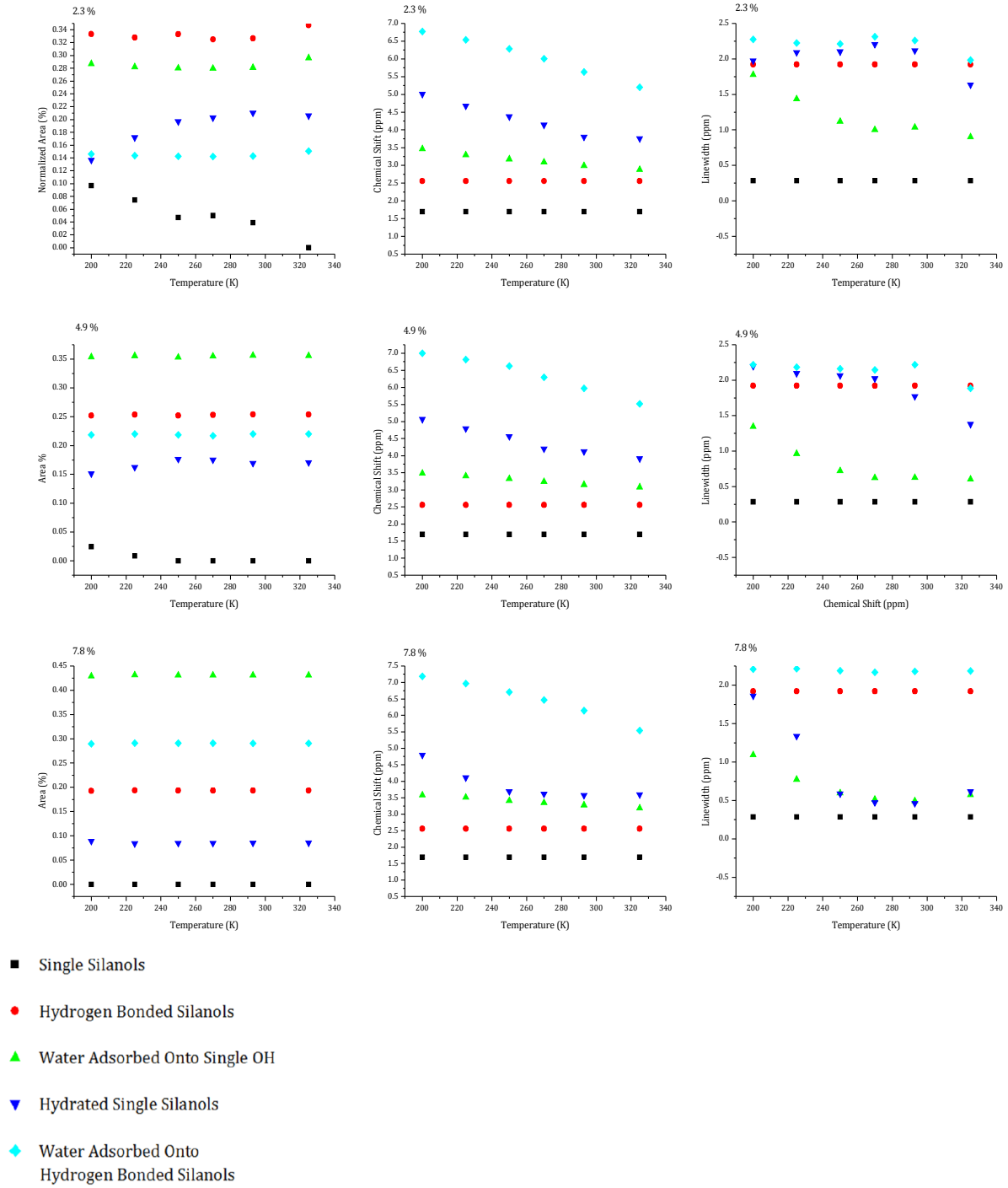

Fig 6.6: Temperature dependance of the fitted parameters. Only 7 parameters were varied.

6.3 Discussions

The elucidation of the spectral features of hydrated MCM-41 has remained a difficult task. Specifically, assignment of the hydroxyl group and water resonances becomes non trivial due to overlapping of the lines. The newly proposed model based on chemical shift averaging due to water molecule surface dynamics within the MCM-41 framework can be used to decompose the spectrum of hydrated (< 0.2 ML) MCM-41. The model is able to assign and track the behaviour across all hydration levels and temperatures studied for the six spin groups (single and hydrogen bonded silanol groups in their hydrated and unhydrated forms as well as the two associated water groups) that are involved, without the addition of magnetization exchange. This demonstrates that an interpretation based on the proposed chemical shift averaging can be used to explain the data and that the concept of magnetization exchange is unnecessary.

6.3.1 Spectra in unhydrated MCM-41

The details regarding experimental ^{1}H NMR results are now discussed in terms of the above model, which was presented in the previous section. It is useful to first characterize the dry sample prior to discussing the hydrated samples. The spectra in dry MCM-41 have been deconvolved into two Lorentzian lines. The assignment of the peaks has been well investigated[3][28] with the narrow resonance centered at ~ 1.75 ppm

assigned to single silanols and the broad resonance at ~ 2.7 ppm assigned to hydrogen bonded surface groups. The deconvolved unhydrated spectra at all temperatures and their associated parameters can be found in Figure 6.7 and Table 6.1 respectively. After correction for Curie's Law the areas under each curve were found to be constant with temperature confirming that the number of protons in the sample wasn't changing during the experiment. This was also confirmed by weighing the sample before and after each temperature run for every level of hydration. Of the total silanol population it was found that 62% are hydrogen bonded and 38% are isolated single silanol groups. Using the known surface area (1132 m^2/g), the surface silanol density was calculated by determining how much signal results from a known number of water protons and was found to be 3.3 OH/nm^2. This value is in good agreement with previously reported values [1][28][36].

Temperature (K)	Single Silanol Parameters			Hydrogen Bonded Silanol Parameters		
	Area (%)	Center (ppm)	Width (ppm)	Area (%)	Center (ppm)	Width (ppm)
200	0.37	1.67	0.27	0.63	2.58	1.94
225	0.37	1.71	0.27	0.63	2.66	1.88
250	0.36	1.75	0.27	0.64	2.68	1.87
270	0.36	1.78	0.27	0.64	2.73	1.85
293	0.34	1.80	0.27	0.66	2.69	1.93
325	0.37	1.82	0.29	0.63	2.77	1.71

Table 6.1: Fitting parameters for the dry unhydated MCM-41 spectra. The spectra were fitted to two Lorentzian lines representing hydrogen bonded and single OH groups.

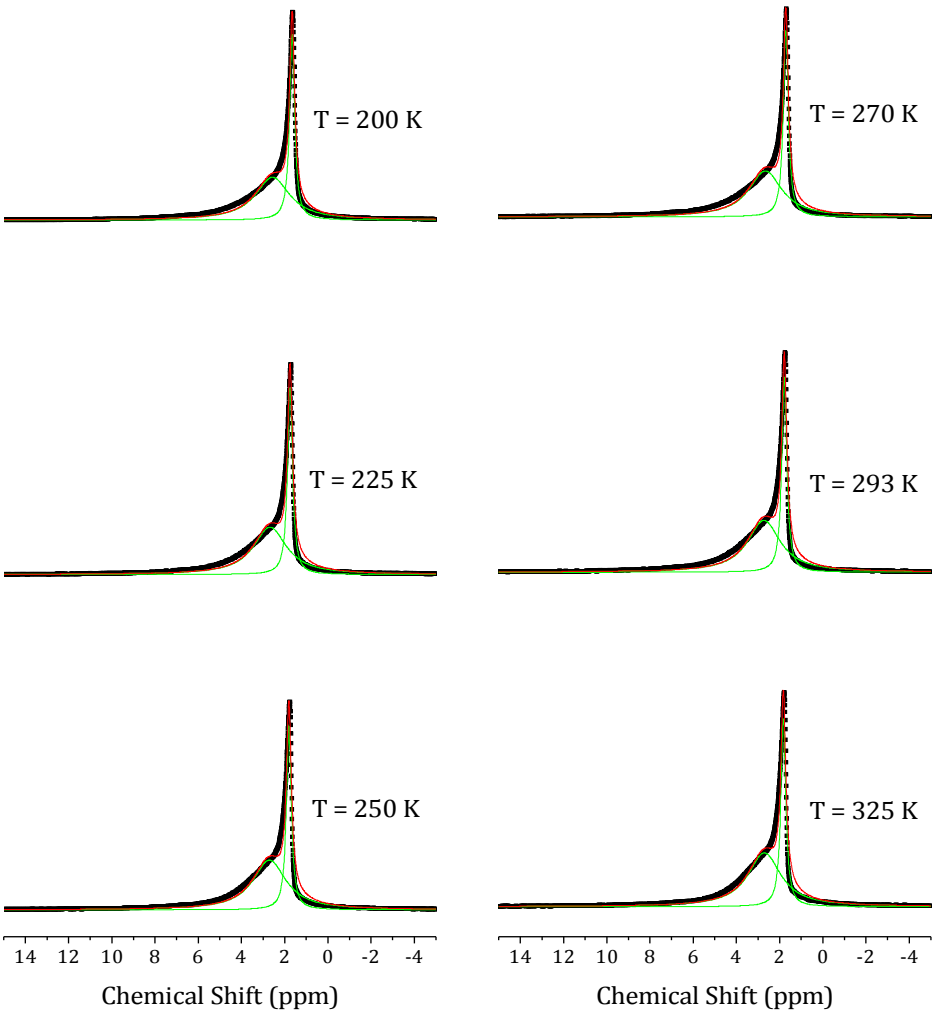

Fig 6.7: Deconvolved ^{1}H MAS NMR spectra for unhydrated MCM-41. The data are shown in black, fitted curve in red, and deconvolved peaks representing hydrogen bonded and single silanol peaks are shown in green.

The calculated areas for the unhydrated single and unhydrated hydrogen bonded groups at each temperature were used as fitting parameters for the hydrated spectra. The calculated area for the hydrogen bonded groups is thought to remain unchanged due to the hydration constraints which have been imposed and has been fixed during the entire fitting process for all data. The single silanol area serves as the starting point to which all subsequent hydrated spectra are compared. The area which has shifted away from ~1.75ppm (see section 6.3.2) defines the area under the resonance of the hydrated single silanols. Using the fact that a known amount of protons gives rise to a known amount of NMR signal one can determine the ratio of water-molecules to the number of shifted protons (discussed in the next section). The centers and linewidths for each line were found to vary only slightly with temperature as expected and is consistent with previous findings [26] (see section 6.2.5).

Since the details of unhydrated line-shapes to a first approximation remain unchanged, the changes in these parameters with temperature and hydration are not of importance when considering the overall picture of hydration at fractional monolayer coverages. Instead the unhydrated results serve more to characterize the sample in terms of ratio of hydrogen bonded to single silanol groups and their respective line-shape areas as well as to determine the approximate surface silanol density.

6.3.2 Hydrated Spectra in MCM-41

The motion induced chemical shift averaging model is able to fit all data across all temperatures and hydrations studied as shown in Figure 6.8. Figure 6.9 shows the deconvolution for one particular case identifying the various peaks. The fitted parameters are shown in Figures 6.10 and 6.11. The model proposes several details regarding the interpretation of fitted spectra and the corresponding parameters which are discussed in detail in the sections to follow. These include calculation of the visiting parameter at each temperature and hydration level studied, confirmation that the chemical shifts for hydrogen bonded protons vary linearly with temperature, and the idea that the water group will always be seen partitioning itself into two groups of 62% and 38%. In addition, the possible hydrogen bonding conformations which are giving rise to observed line shapes can be determined by observing the changes in the chemical shifts and linewidths for each spin groups. It is thought that the rearrangement of water molecules on the surface takes place as a result of increasing hydration level, whereas increasing temperature simply increases the thermal energy and hence the visiting parameter and not the conformations which are being sampled.

6.3.3 The Visiting Parameter

The visiting parameter is determined through the ratio of the number of water molecules to the number of shifted single silanol protons as per equation 6.1. Table 6.2 shows the corresponding visiting parameters for the spectra shown in Figure 6.8. The proposes that this parameter should vary linearly with hydration at a fixed temperature with hydration which was found not to be the case. This suggests that the water-water interactions are important since non-linear surface coverage as a function of hydration (temperature fixed) is indicative of cooperative nature between the water molecules. It was also interesting to find that the number of shifted single silanols displays a linear decrease with increasing temperature at a given hydration level. In general the dependance is not expected be linear. If we consider the water molecule to undertake a random walk on the surface then the number of OH's visited is proportional to the area covered by the molecule on the experimental timescale. This area is proportional to the square of the distance travelled on this time scale. This distance can be related to the diffusion coefficient for 2-D diffusion:

$$\langle r^2 \rangle = 4\,t\,D_s \qquad 6.5$$

In various systems D_s is seen to increase with temperature according to the Arrhenius Law $\left(D_s \propto e^{-E_a/RT}\right)$ so that the number of OH's visited could be expected to increase

exponentially with decreasing values of $1/T$. The above observed linear behaviour for the visiting parameter with T may be the result of the small range of temperature (200 K-325K) covered in this study.

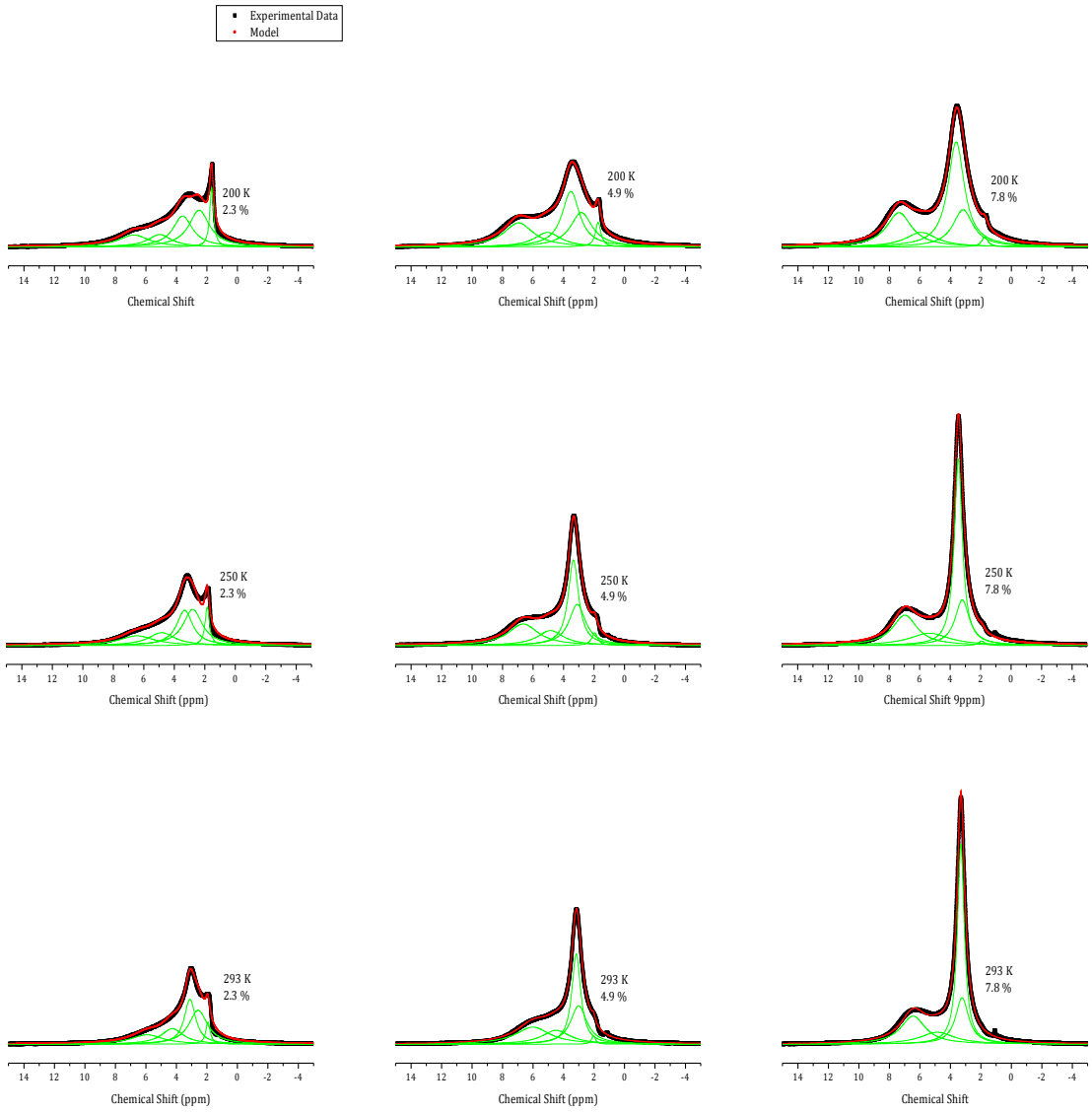

Fig 6.8: Modelled ^{1}H NMR spectra (experimental in black and deconvolution in green) for hydrated MCM-41. The experimental data is well represented at all hydrations and temperatures.

T = 250 K
2.3% Hydration

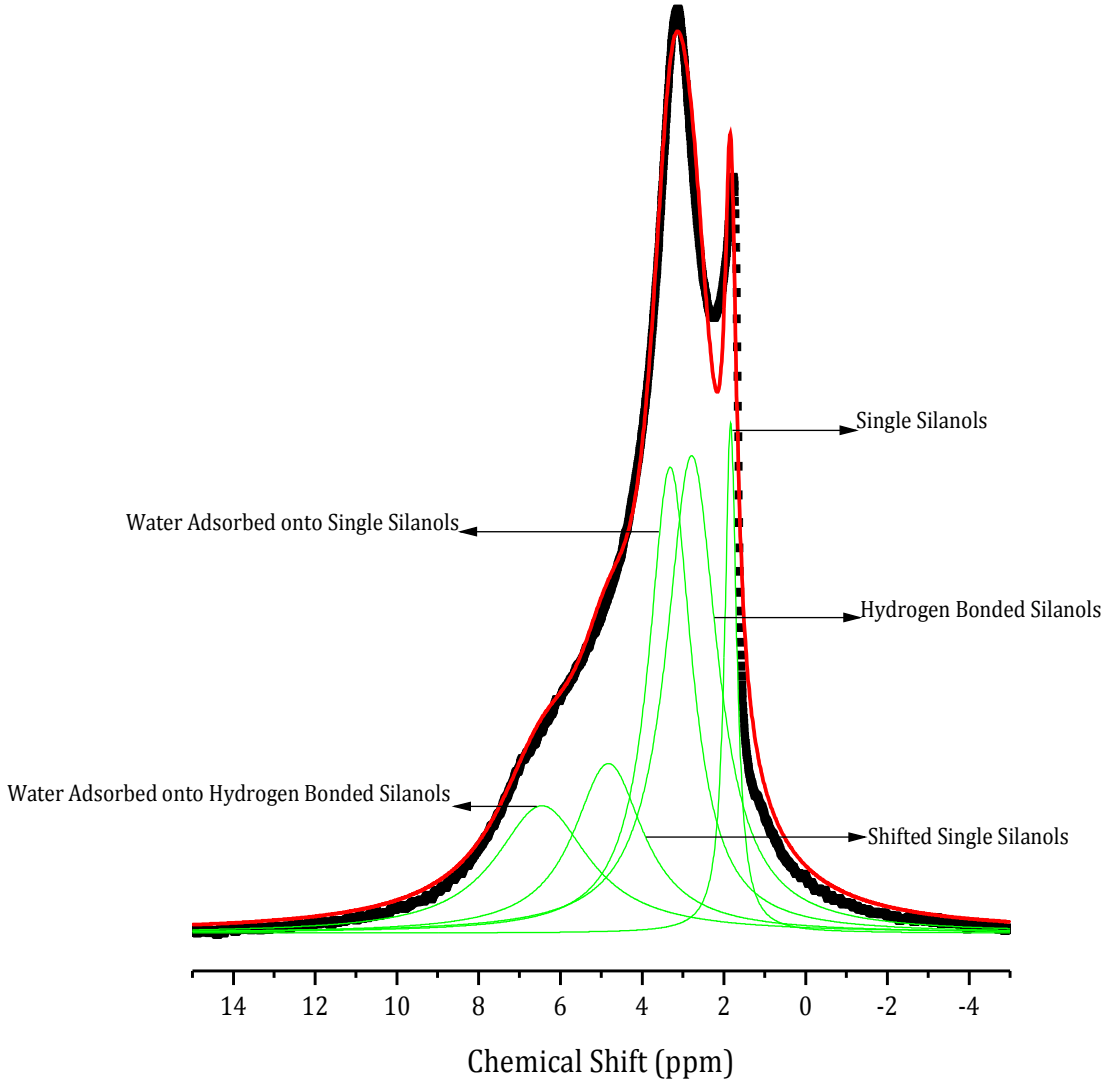

Fig 6.9: Deconvolved spectrum of hydrated MCM-41 for T = 250 K and 2.3 % hydration using the model presented. Shown are the identifications of the five peaks (green). The actual fit is shown in red and the raw experimental data are represented by black squares.

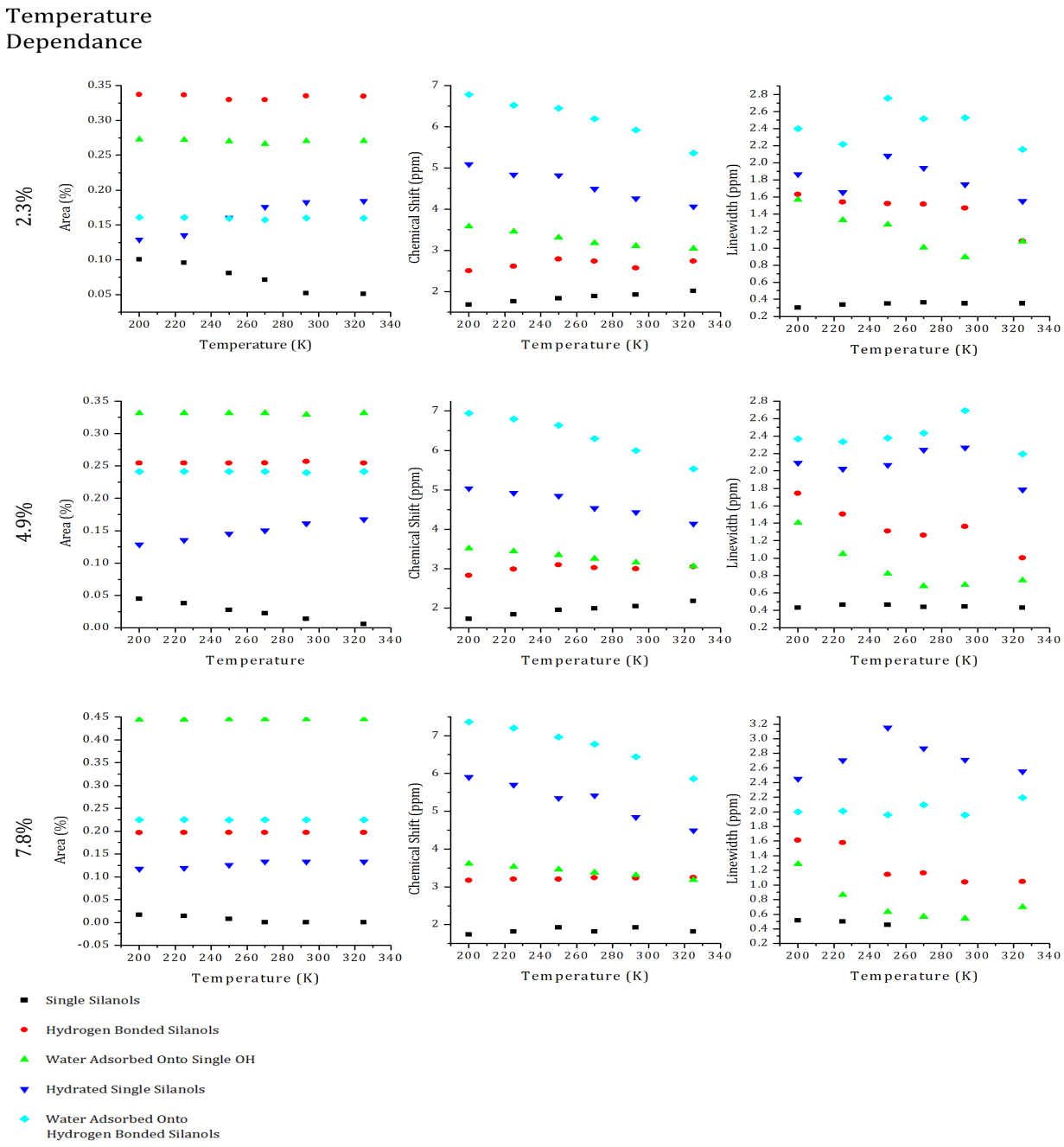

Fig 6.10: Temperature dependance of the parameters which describe the five spin groups for all temperatures studied are shown for hydration levels of 2.3%, 4.3%, and 7.8%. Both the chemical shift and visiting parameters were found to vary linearly with temperature.

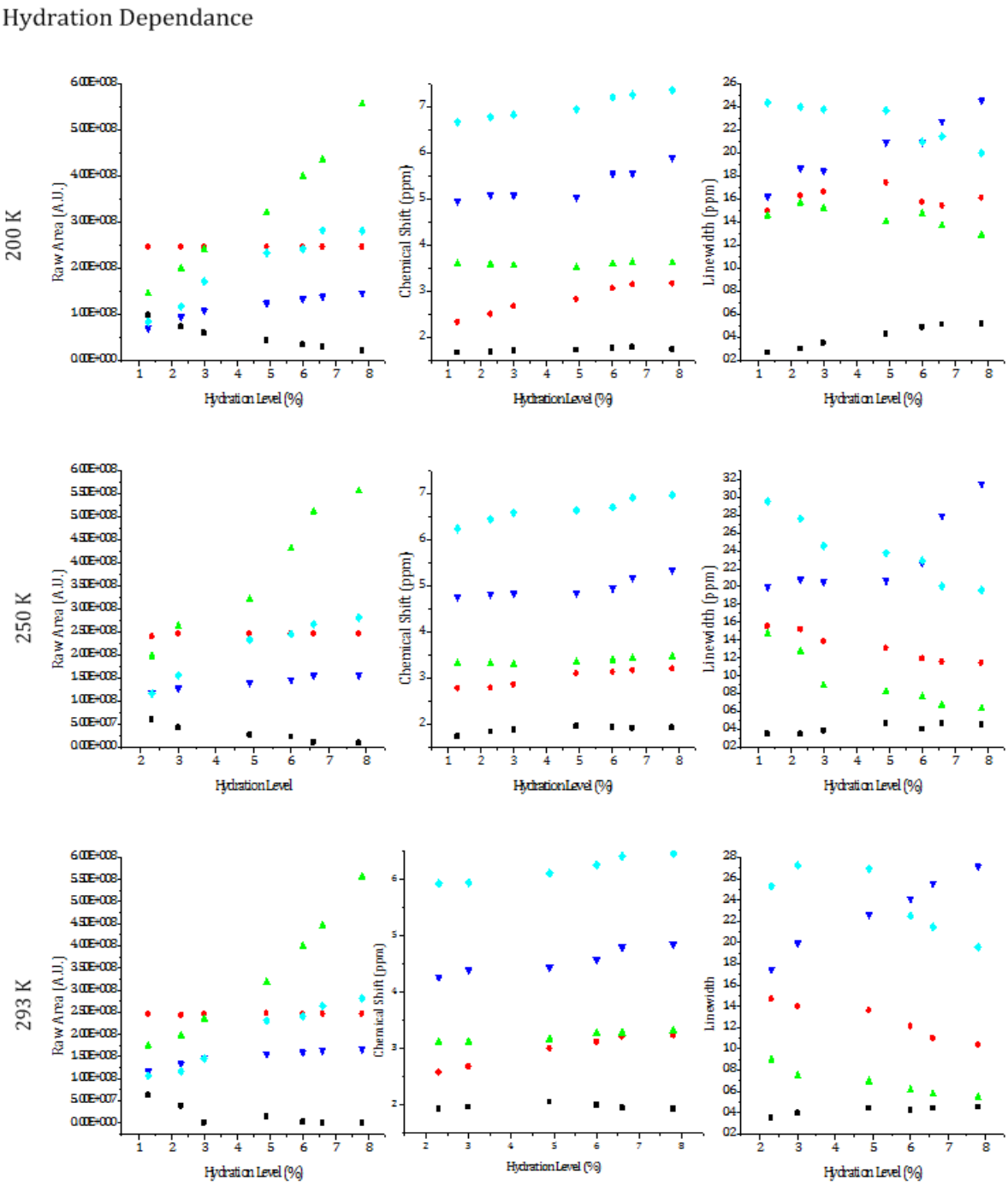

Fig 6.11: Hydration dependance of the parameters which describe each of the five spin groups at temperatures of 200 K, 250 K, and 293 K.

Hydration Level	T = 200 K	T = 250 K	T = 293 K
2.3%	0.95	1.18	1.35
4.9%	0.78	0.91	0.98
7.8%	0.53	0.56	0.59

Table 6.2: Visiting parameters at different temperatures and hydrations.

6.3.4 Assignment of the Water Groups.

The areas of all peaks at all temperatures are well defined. For the hydrated single silanol peak this area simply is the area which has disappeared from its original unhydrated position at ~1.75ppm. The hydrogen bonded area was kept constant throughout the entire fitting process. This appears to be a reasonable approximation. Indeed two water peaks are present in the spectra of hydrated MCM-41 which together define the total water area. The water group associated with the higher chemical shift consistently represents 37-42% of the area of the water resonance and also shows a broader linewidth across all temperature and hydrations. These features are in keeping with what is expected from the water group hydrating the single silanols, while in the process bridging via its two protons in order to get such a high chemical shift value. Accordingly the associated chemical shift for the hydrated single silanol group should be quite low since this implies an increase in p_C. However this chemical shift is quite high as

well and what complicates matters more is that this shift is seen to increase while the chemical shift of the high ppm water peak increases as well. This trend precludes any possible assignment of this peak to water hydrating the single silanol groups.

An alternate interpretation is proposed in which each single silanol group presents three hydrogen bonding sites (the hydrogen and the two free obitals of the oxygen) whereas a given silanol group involved in a hydrogen bond presents only one. Loosely speaking this effectively increases the single silanol hydration area available for water by a factor of 3. This would lead to 66% of water molecules being associated with single silanol groups and 33% with the hydrogen bonded groups. Furthermore the decreased coordinations available to the water molecules adsorbed to hydrogen bonded hydroxyls allow for the highest possible chemical shifts to occur for the protons involved, as bridging to two separate oxygen atoms occurs. Also recall that the chemical shift of the hydrogen bonded hydroxyl group protons are not assumed to be affected by hydrogen bonding. Consequently the water group associated with the high chemical shift is assigned to water hydrating the hydrogen bonded silanols.

The water peak which was found to represent consistently 63-58% percent of the total water area is assigned to water hydrating the single silanol groups. This proposed hydration scheme would explain the chemical shift values for both hydrated single silanols and the associated water.

6.3.5 Chemical Shifts of Hydrogen Bonded Protons.

Figure 6.10 diagrams the chemical shifts as a function of temperature for hydration levels of 2.3, 4.9, and 7.8 %. Linear trends are observed supporting the earlier findings[38][39] which report the chemical shift of hydrogen bonded protons in silica-water systems to vary linearly with temperature. In light of the model presented here the same behaviour has now been confirmed for the water-MCM-41 system. Furthermore, this leads one to the interpretation that the conformations accessed by a group of water molecules do not change with temperature at a fixed hydration but rather the hydrogen bonding strengths in each conformation change. This is consistent with the fact that water molecules are still undergoing liquid like motion at 200 K [28] and thus each is still able to visit a number of sites.

The variations of chemical shift due to hydration are thought to be dominated by rearrangement of the water molecules into different fractional probabilities p_N. The same trend of an increasing chemical shift is observed for both types of hydrated silanol groups and the two water groups. The hydrated single silanol groups experience only a small change in the average chemical shift value whereas the corresponding water sees a more pronounced effect with hydration. Likely, this is caused by an increased number of water protons which are hydrogen bonded to the surface which is a result of more water molecules forming two hydrogen bonds to the surface. If one closely examines Figure 6.3 one will notice that the value of the chemical shift associated with hydrated single silanols does not depend on water forming bridges between. The value actually strictly depends on

the fractional probability of finding the proton involved in a hydrogen bond. The water assigned to the hydrogen bonded OH groups also shows similar features and is also thought to be undergoing rearrangement into the bridge structure. In summary, it is proposed the water molecules hydrating the MCM-41 surface at low hydrations undergo a rearrangement in their average hydrogen bonding conformations due to changes in hydration. This observation leads to the suggestion that rearrangement of water on the surface into bridges with increasing hydration is the precursor for monolayer formation.

6.3.6 The Linewidths

Only the linewidth of protons of water adsorbed onto single OH groups exhibits a clear trend with respect to temperature; a broadening of the lines as temperature is decreased. This is expected to come about because the water involved is moving too fast for this proton resonance to be affected by MAS at 10 kHz. Hence, the line broadens with decreasing temperature due to a decrease in motional averaging of the water dipole-dipole interaction. The remaining observed linewidths show complex behaviour with temperature at different hydration levels. These observations are not understood at this time, may be scatter due to temperature, and are topics for future investigation.

The behaviours of the linewidths as a function of hydration however are readily explained in terms of the ideas presented in section 6.2.5. The width of the line associated with the single silanol group shows a general increase with hydration. In keeping with

previous conclusions, the reason for this behaviour comes from the idea that as the hydration level is increased rearrangement of the water molecules into more bridge conformations, including that of Fig. 6.3 e, occurs.

The linewidth of the water group associated with hydrogen bonded silanols clearly shows a decreasing trend as the hydration level is increased. The previous conclusions regarding the trends of the increasing chemical shift for this water group with increasing hydration support the idea that indeed the water molecules are collapsing more and more into one conformation. This is consistent with the idea that if water molecules are adopting only one of the conformations proposed the associated chemical shift distribution should decrease due to increasing environmental similarities between each water molecule in this group.

CHAPTER 7

Conclusions

Before this work was concluded the features and origins of the spectral line shapes associated with hydrated MCM-41 at fractional monolayer coverages have been attributed to various types of magnetization exchange processes. Furthermore, such interpretations have provided limited insight into the behaviour of water molecules as function of temperature or hydration.

In this work a model is proposed where chemical shift averaging occurs through water molecule surface dynamics. The results have shown that magnetization exchange processes are negligible when describing hydrated MCM-41 spectra at low hydrations. The model reproduces all spectral line shapes at every hydration and temperature studied with a clear definition and interpretation of the associated spectral decomposition.

Some interesting aspects of how water molecules wet the surface of MCM-41 have been brought into light based on the interpretations of the model. Firstly it was confirmed that as the temperature is increased at fixed hydration water molecules show a linear variation in their ability to visit different hydroxyl groups. As the hydration is increased at fixed

temperature it was found that a non-linear increase in the number of hydrated silanol species occurred. This is evidence that as the hydration level is increased (while maintaining fractional surface coverage), water molecules do undergo a cooperative type of hydration of the surface.

Secondly two water groups were identified of which one represents 37%-42% of the total water and was assigned to water adsorbed onto the hydrogen bonded surface groups. It was found that the water groups essentially maintained the expected fractions (33% and 66%) over all temperatures and hydrations with minor deviations. The conclusion that can be drawn is that water molecules do not preferentially hydrate single or hydrogen bonded silanol groups but rather see a surface which statistically has three times more hydration sites arising from the single silanol groups than their hydrogen bonded counterpart.

Thirdly, the variations of the chemical shift with temperature were found to be linear and were thus attributed simply to changes in the hydrogen bond strength of each conformation and not changes in the probability for each conformation to occur. This finding suggests that protons involved in hydrogen bonding in the MCM-41 nanostructure at low hydrations do not rearrange themselves into different conformations due to temperature. The chemical shift variation of the water groups with increasing hydration is thought to arise due to rearrangement of the water molecules on the surface into more bridge structures in which each water is involved in two hydrogen bonds. Therefore it is concluded that as the surface sites fill up a precursor to the formation of a monolayer is the bridging of water molecules between the silanol groups.

Lastly, the associated linewidths show a complex character which is still not completely

understood. However, certain trends did emerge which support previous conclusions regarding the rearrangement of water as a function of hydration. Overall a general broadening is observed as temperature is decreased as expected if dipolar coupling is not completely removed by MAS . It may be noted that one does not know a priori how the linewidths should vary since the linewidth itself is due to a combination of chemical shift distribution and broadening due to dipolar coupling.

In summary, the proposed model based on chemical shift averaging resulting from rotational motion and self-diffusion of water molecules is able to reproduce the experimental data across all hydration and temperatures without the need for magnetization exchange to occur. Additionally insights into water monolayer formation on the MCM-41 surface and the hydrogen bonding details as functions of temperature and hydration were provided as a result of such an interpretation.

Recommendations for future work include investigating hydration levels beyond 0.2 monolayers (hydroxyl proton to water molecule ratio of 1:1) in order to shed more light on the pore-filling process. The present low hydration model would serve as the basis for modelling results at high hydration.

The University of Waterloo has access to Sharcnet and in this connection it would be useful to carry out large scale molecular dynamics simulations as well as perform “large” ab-initio calculations using slab like geometries such as cristobalite for the substrate. It is thought that these calculations can yield better estimates of the chemical shifts of hydrogen bonded protons in various water molecule – surface OH conformations.

Preliminary deuteron studies involving two different sources of MCM-41 at low

hydrations have shown differences in the water deuteron NMR spectra, which are thought to be attributed to differences in the surface silanol density of MCM-41. Thus proton NMR involving MCM-41 should be done in order to confirm this result using the interpretations supplied by the present model.

APPENDICES

Appendix I: Fitted Spectra (11 adjustable parameters)

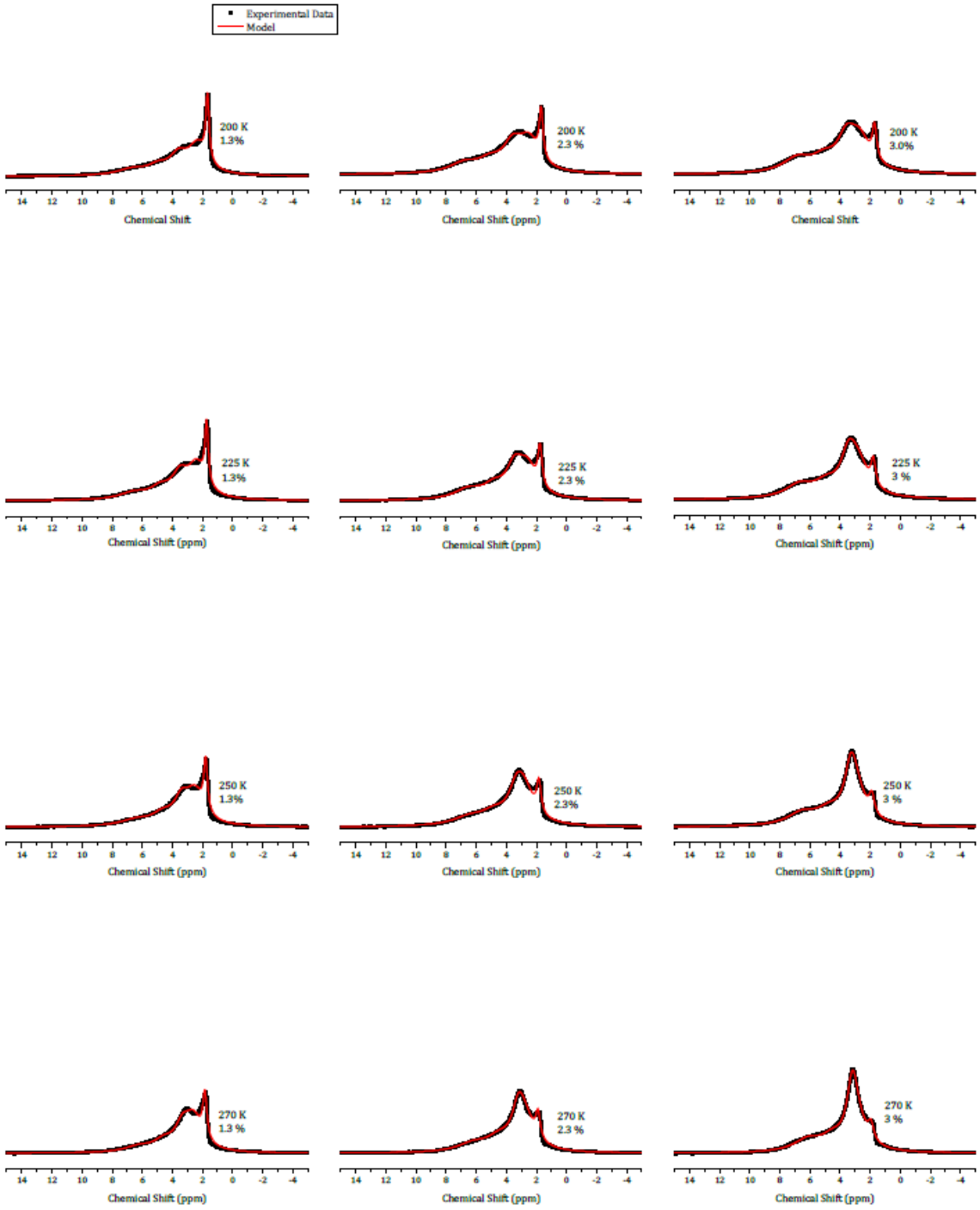

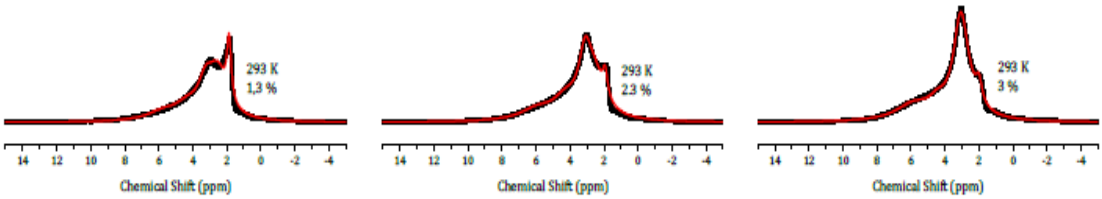
293 K
1,3 %
293 K
2.3 %
293 K
3 %
14 12 10 8 6 4 2 0 -2 -4
Chemical Shift (ppm)

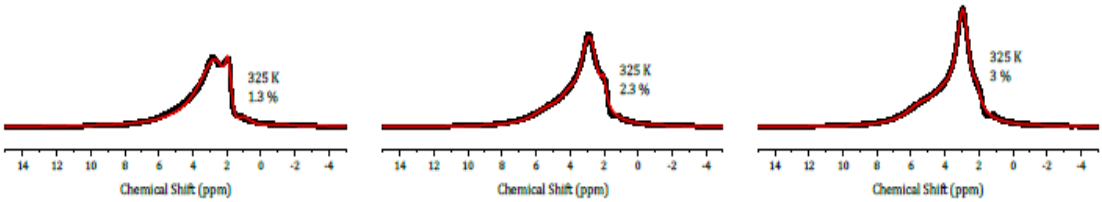
325 K
1.3 %
325 K
2.3 %
325 K
3 %
14 12 10 8 6 4 2 0 -2 -4
Chemical Shift (ppm)

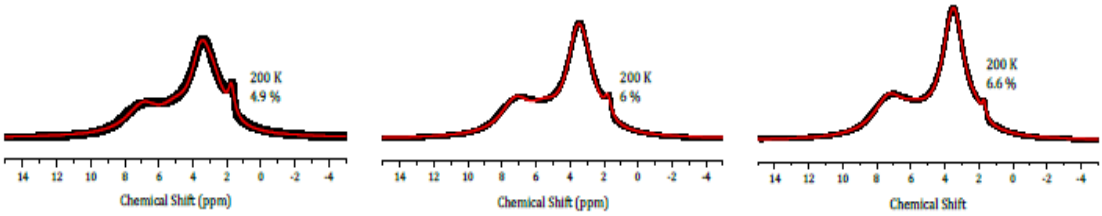
200 K
4.9 %
200 K
6 %
200 K
6.6 %
14 12 10 8 6 4 2 0 -2 -4
Chemical Shift (ppm)
Chemical Shift

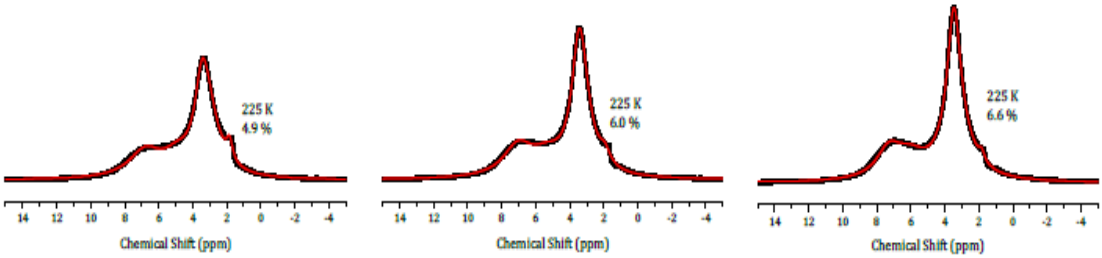
225 K
4.9 %
225 K
6.0 %
225 K
6.6 %
14 12 10 8 6 4 2 0 -2 -4
Chemical Shift (ppm)

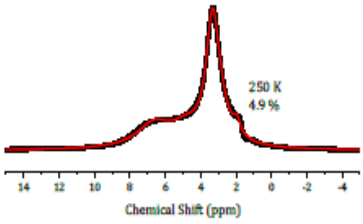
250 K
4.9 %
14 12 10 8 6 4 2 0 -2 -4
Chemical Shift (ppm)

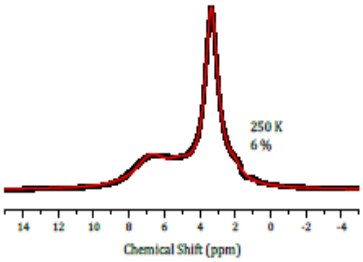
250 K
6 %
14 12 10 8 6 4 2 0 -2 -4
Chemical Shift (ppm)

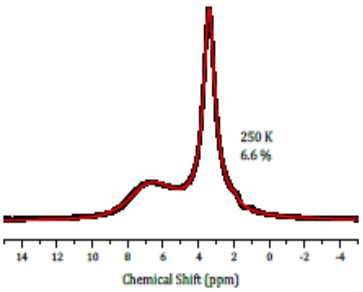
250 K
6.6 %
14 12 10 8 6 4 2 0 -2 -4
Chemical Shift (ppm)

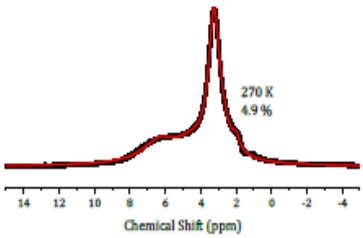
270 K
4.9 %
14 12 10 8 6 4 2 0 -2 -4
Chemical Shift (ppm)

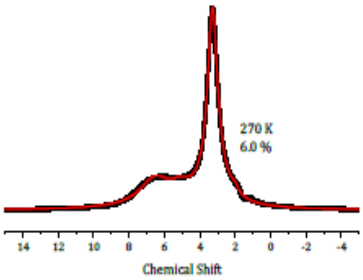
270 K
6.0 %
14 12 10 8 6 4 2 0 -2 -4
Chemical Shift

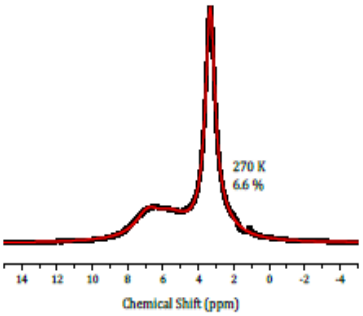
270 K
6.6 %
14 12 10 8 6 4 2 0 -2 -4
Chemical Shift (ppm)

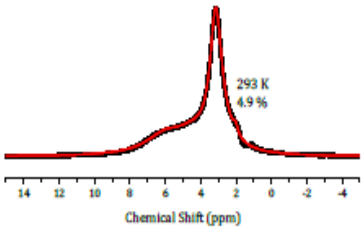
293 K
4.9 %
14 12 10 8 6 4 2 0 -2 -4
Chemical Shift (ppm)

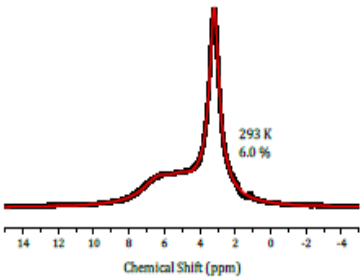
293 K
6.0 %
14 12 10 8 6 4 2 0 -2 -4
Chemical Shift (ppm)

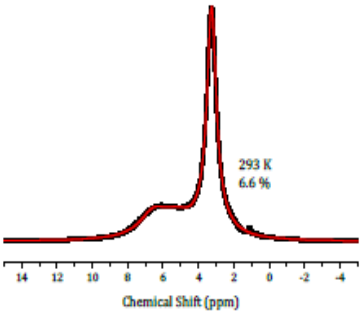
293 K
6.6 %
14 12 10 8 6 4 2 0 -2 -4
Chemical Shift (ppm)

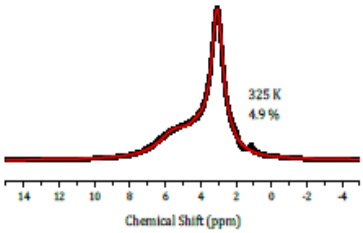
325 K
4.9 %
14 12 10 8 6 4 2 0 -2 -4
Chemical Shift (ppm)

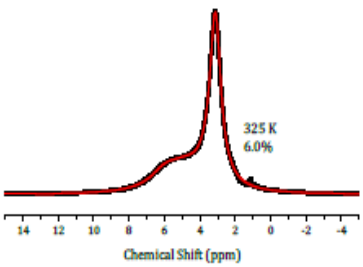
325 K
6.0%
14 12 10 8 6 4 2 0 -2 -4
Chemical Shift (ppm)

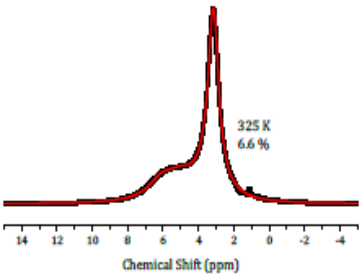
325 K
6.6 %
14 12 10 8 6 4 2 0 -2 -4
Chemical Shift (ppm)

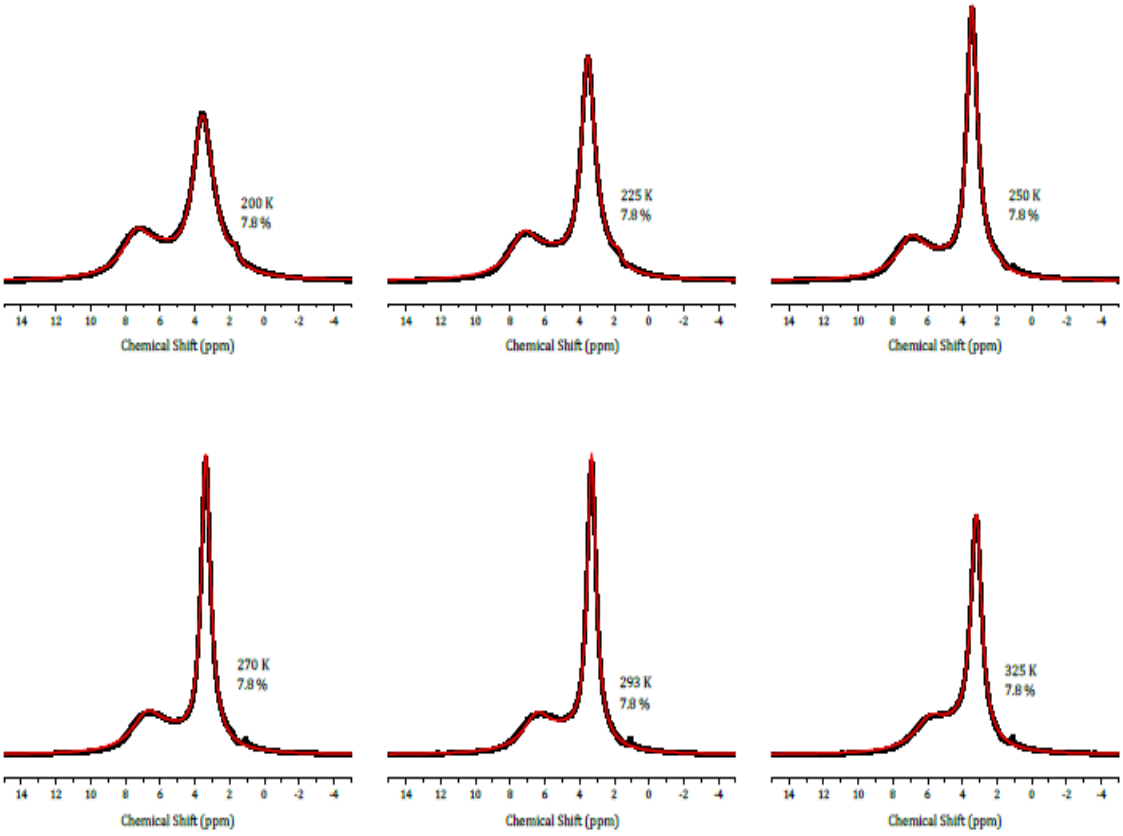
200 K
7.8 %
225 K
7.8 %
250 K
7.8 %
270 K
7.8 %
293 K
7.8 %
325 K
7.8 %
14 12 10 8 6 4 2 0 -2 -4
Chemical Shift (ppm)

Appendix II: Fitted Spectra (7 adjustable parameters)

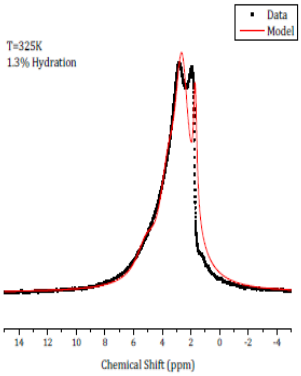

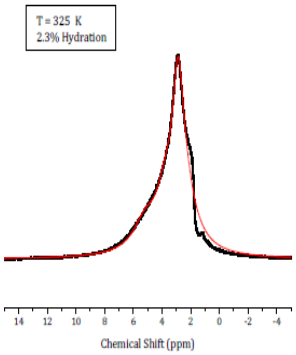

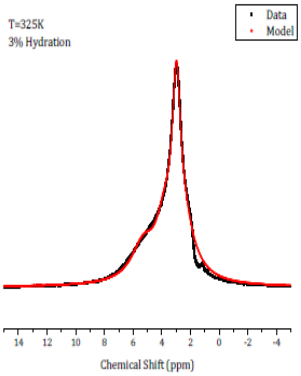

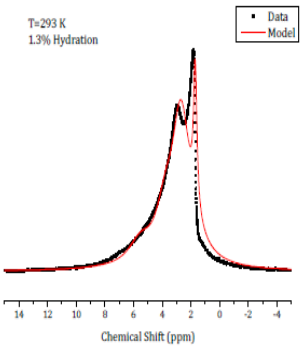

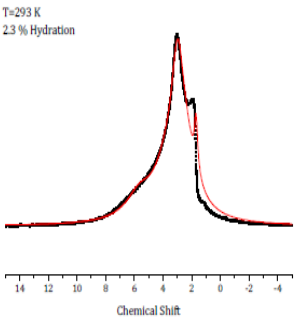

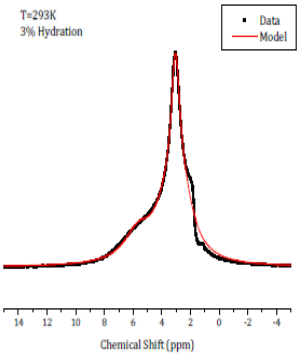

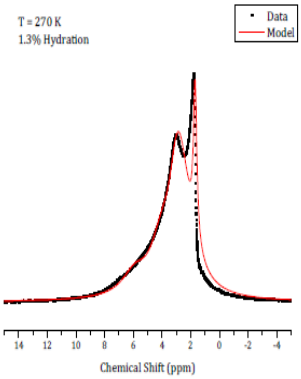

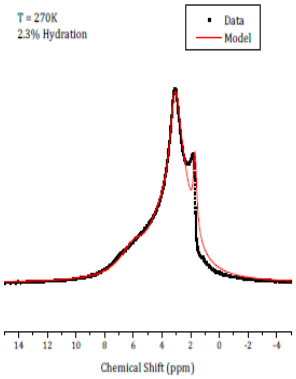

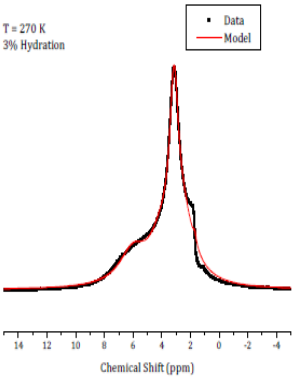

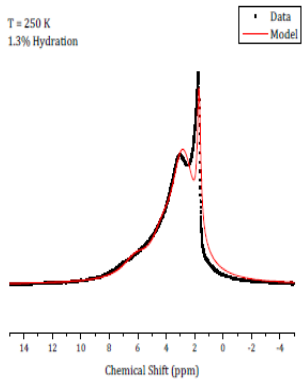
T = 250 K
1.3% Hydration
Data
Model
14 12 10 8 6 4 2 0 -2 -4
Chemical Shift (ppm)

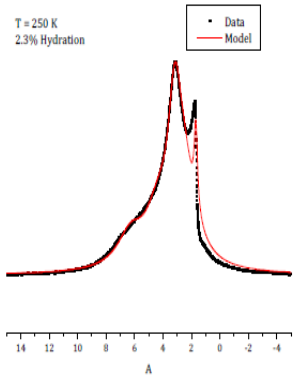
T = 250 K
2.3% Hydration
Data
Model
14 12 10 8 6 4 2 0 -2 -4
A

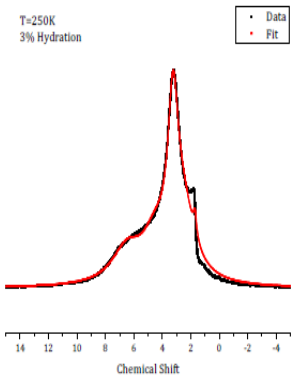
T=250K
3% Hydration
Data
Fit
14 12 10 8 6 4 2 0 -2 -4
Chemical Shift

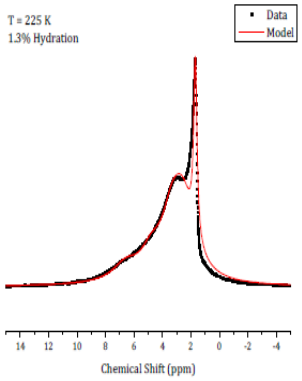
T = 225 K
1.3% Hydration
Data
Model
14 12 10 8 6 4 2 0 -2 -4
Chemical Shift (ppm)

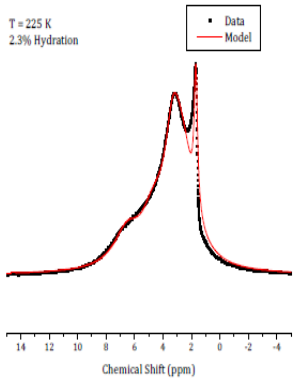
T = 225 K
2.3% Hydration
Data
Model
14 12 10 8 6 4 2 0 -2 -4
Chemical Shift (ppm)

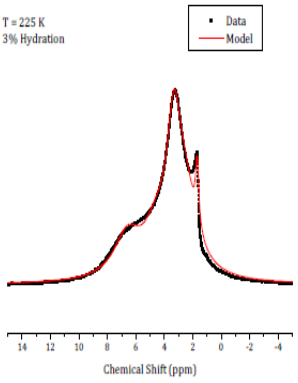
T = 225 K
3% Hydration
Data
Model
14 12 10 8 6 4 2 0 -2 -4
Chemical Shift (ppm)

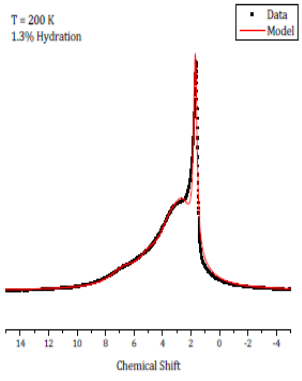
T = 200 K
1.3% Hydration
Data
Model
14 12 10 8 6 4 2 0 -2 -4
Chemical Shift

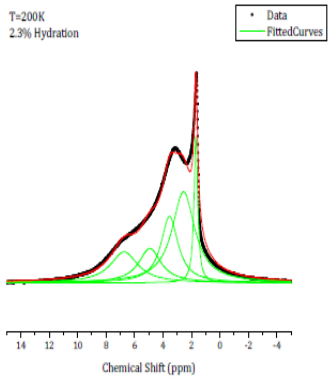
T=200K
2.3% Hydration
Data
FittedCurves
14 12 10 8 6 4 2 0 -2 -4
Chemical Shift (ppm)

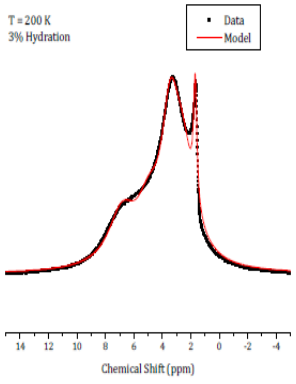
T = 200 K
3% Hydration
Data
Model
14 12 10 8 6 4 2 0 -2 -4
Chemical Shift (ppm)

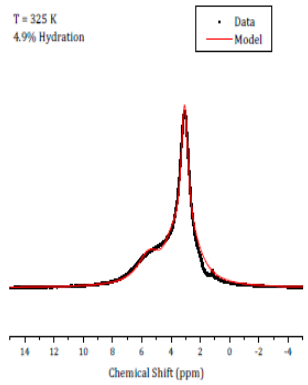
T = 325 K
4.9% Hydration
Data
Model
14 12 10 8 6 4 2 0 -2 -4
Chemical Shift (ppm)

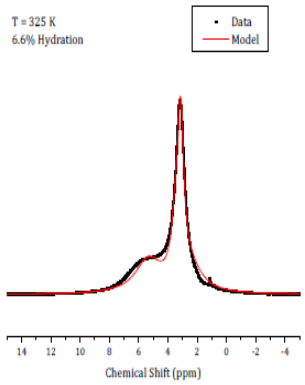
T = 325 K
6.6% Hydration
Data
Model
14 12 10 8 6 4 2 0 -2 -4
Chemical Shift (ppm)

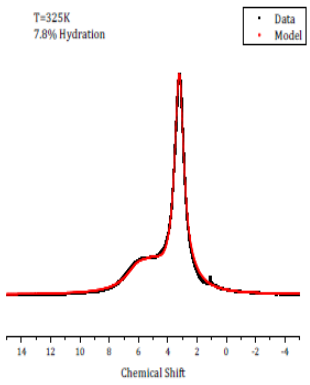
T=325K
7.8% Hydration
Data
Model
14 12 10 8 6 4 2 0 -2 -4
Chemical Shift

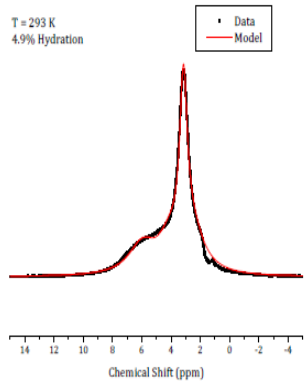
T = 293 K
4.9% Hydration
Data
Model
14 12 10 8 6 4 2 0 -2 -4
Chemical Shift (ppm)

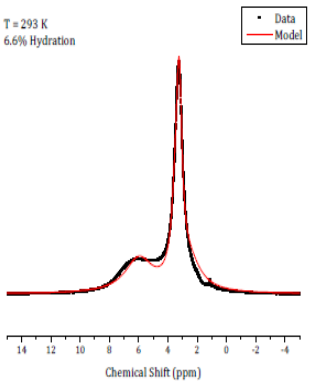
T = 293 K
6.6% Hydration
Data
Model
14 12 10 8 6 4 2 0 -2 -4
Chemical Shift (ppm)

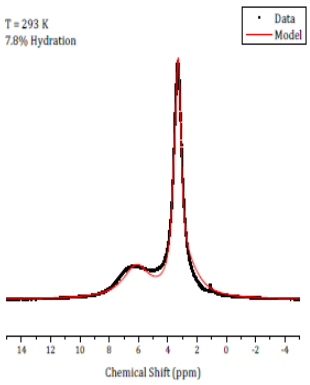
T = 293 K
7.8% Hydration
Data
Model
14 12 10 8 6 4 2 0 -2 -4
Chemical Shift (ppm)

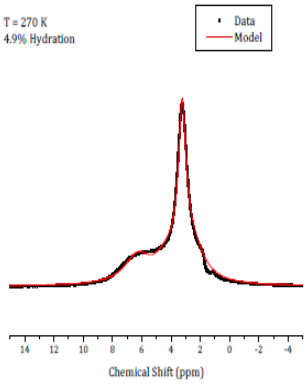
T = 270 K
4.9% Hydration
Data
Model
14 12 10 8 6 4 2 0 -2 -4
Chemical Shift (ppm)

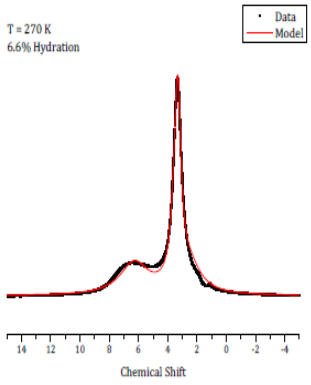
T = 270 K
6.6% Hydration
Data
Model
14 12 10 8 6 4 2 0 -2 -4
Chemical Shift

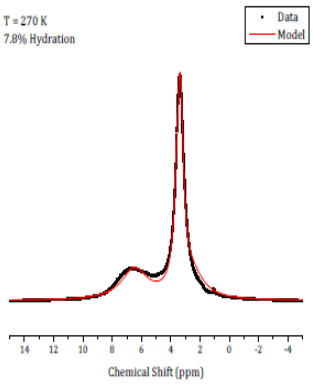
T = 270 K
7.8% Hydration
Data
Model
14 12 10 8 6 4 2 0 -2 -4
Chemical Shift (ppm)

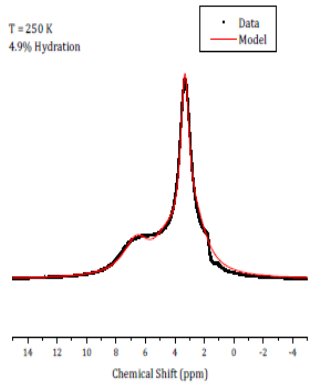
T = 250 K
4.9% Hydration
Data
Model
14 12 10 8 6 4 2 0 -2 -4
Chemical Shift (ppm)

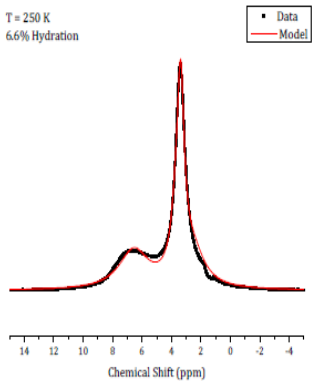
T = 250 K
6.6% Hydration
Data
Model
14 12 10 8 6 4 2 0 -2 -4
Chemical Shift (ppm)

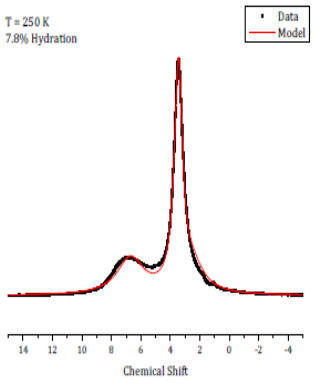
T = 250 K
7.8% Hydration
Data
Model
14 12 10 8 6 4 2 0 -2 -4
Chemical Shift

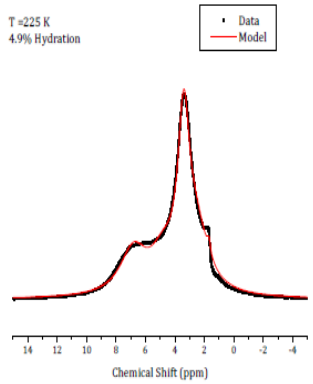
T =225 K
4.9% Hydration
Data
Model
14 12 10 8 6 4 2 0 -2 -4
Chemical Shift (ppm)

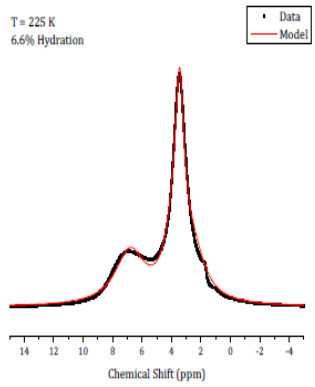
T = 225 K
6.6% Hydration
Data
Model
14 12 10 8 6 4 2 0 -2 -4
Chemical Shift (ppm)

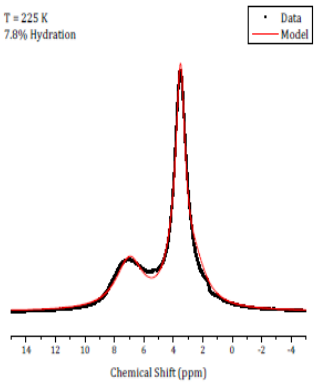
T = 225 K
7.8% Hydration
Data
Model
14 12 10 8 6 4 2 0 -2 -4
Chemical Shift (ppm)

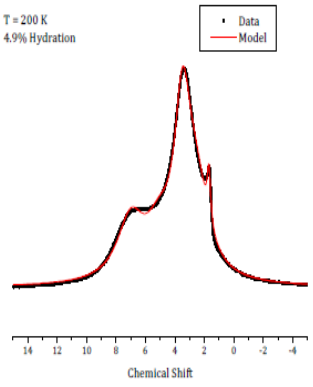
T = 200 K
4.9% Hydration
Data
Model
14 12 10 8 6 4 2 0 -2 -4
Chemical Shift

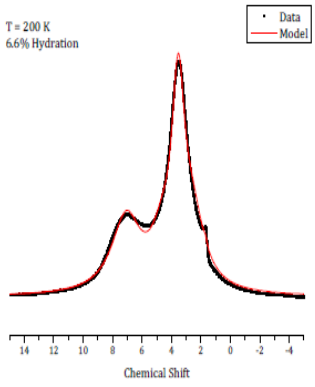
T = 200 K
6.6% Hydration
Data
Model
14 12 10 8 6 4 2 0 -2 -4
Chemical Shift

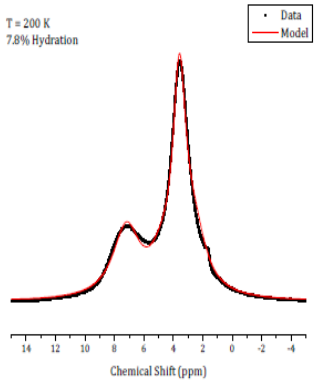
T = 200 K
7.8% Hydration
Data
Model
14 12 10 8 6 4 2 0 -2 -4
Chemical Shift (ppm)

Appendix III: N_2 Adsorption Data

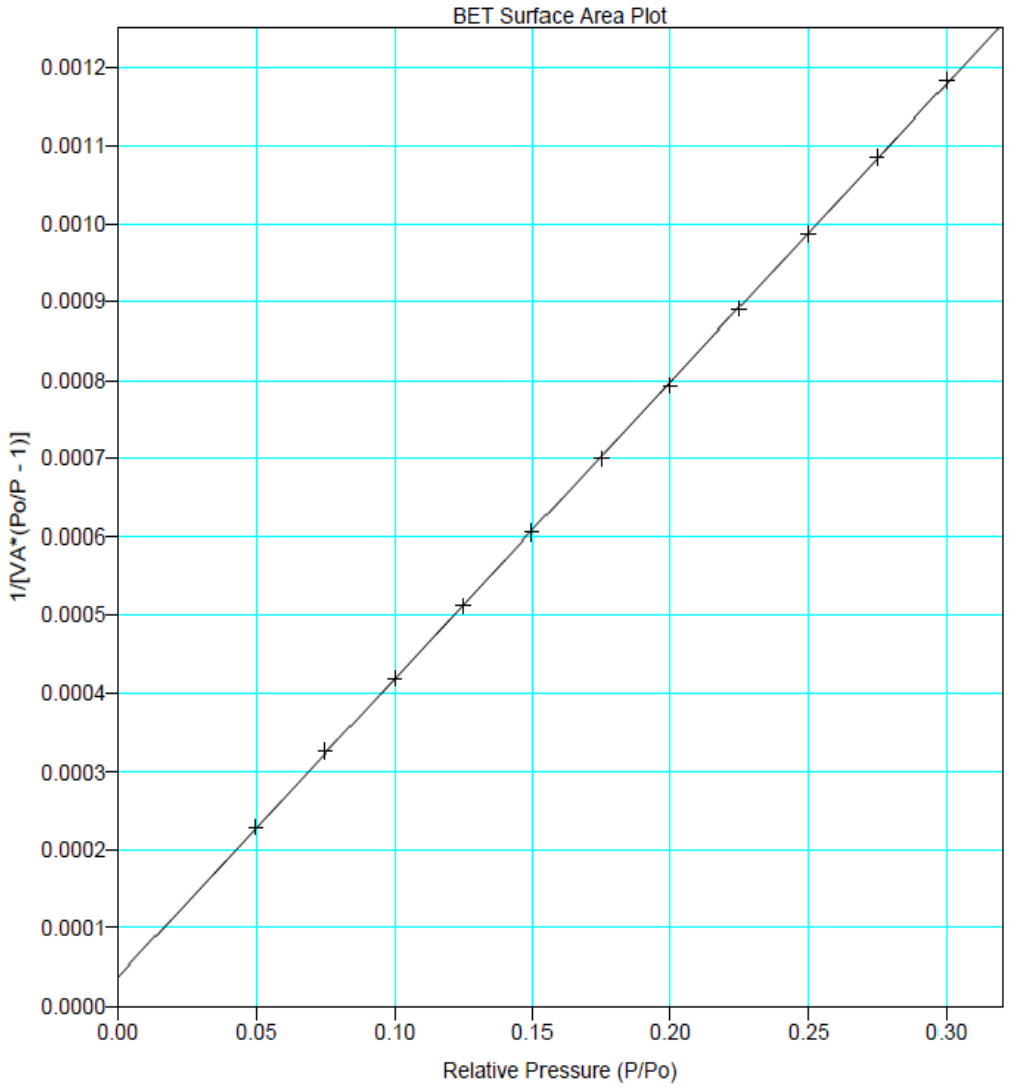

Single Point Surface Area at P/Po 0.29983450 :	1103.3185	m^2/g
BET Surface Area:	1132.8904	m^2/g

Sat. Pressure: 743.26 mmHg
Meas. Freespace: -0.0688 cm^3
Sample Weight: 0.0243 g
Evac. Time: 6.000000 minutes
Equil. Interval: 5 secs

Bibliography

[1] M. Niknam, MSc. Thesis, University of Waterloo (2010)

[2] J. Hassan, PhD Thesis, University of Waterloo (2006).

[3] B. Grunberg, T. Emmler, E. Gedat, I. Shenderovich, G.H. Findenegg, H-H. Limbach, G. Buntkowsky, *J. Chem. Eu.* **10**, 5689 (2004).

[4] F. Bloch, Phys. Rev. **70**, 460 (1946).

[5] C. Slichter, *Principles of Magnetic Resonance,* Ch. 3., Springer-Verlag (1980).

[6] N. Bloembergen, E. Purcell, R. Pound, *Phys. Rev.* **73**, 679 (1948)

[7] M. Cohen, *Solid State Physics,* Vol. 5, p321-438 (1957).

[8] J. Slater, *Phys. Rev.* **36,** 57 (1930)

[9] P. Gill, *Advances in Quantum Chemistry* **25**, 141–205. (1994)

[10] J.S. Beck, J.C. Vartuli, W.J. Roth, M.E. Leonowicz, S.B C.T. Kresge, K.D. Schmitt, C.T-W. Chu, D.H. Olson, E.W.,Sheppard, S.B. McCullen, J.B. Higgins, J.L. Shlenker.,*J. Am. Chem. Soc*., **114**, 10834 (1992).

[11] C.T. Kresge, M.E. Leonowicz, W.J. Roth, J.C. Vartuli, J.S.Beck, *Nature,* **359**,710 (1992).

[12] S. Anandan, M. Okazaki, *Micro. Meso. Materials.* **87**, 77 (2005).

[13] D. Baute, V. Frydman, H. Zimmerman, S. Kababya, D.Goldfarb, *J. Phys. Chem. B*, **109**, 7807 (2005).

[14] J. Chen, Q.Li, H.Ding, W.Pang, R. Xu, *Langmuir*, **13**, 2050 (1997).

[15] Y. Inaki, H. Yoshida, T. Yoshida, T. Hattori, *J.Phys. Chem. B,* **101**, 9098 (2002).

[16] C.Y. Chen. H.X. Li, M.E. Davis, *Micoporous Materials* **2**, 17 (1993).

[17] R. Server, R. Alcala, J. Dumesic, T. Root, *Micro. Meso. Materials.* **77**, 53 (2005)

[18] Image taken from the web.

[19] S. Brunauer, P. Emmett, E. Teller, *J. Am. Chem. Soc*, **60**, 309 (1938).

[20] S. Gregg, K. Sing, *"Adsorption, Surface Area and Porosity"* Academic Press, London (1982).

[21] E. Barrett, L. Joyner, A. Halenda, *Langmuir* **13**, 6267 (1997).

[22] C. Kittel, *Introduction to Solid State Physics,* Wiley 8th ed. (2004).

[23] N. Ashcroft, N. Mermin, *Solid State Physics,* Brooks Cole, 1st edition (1976).

[24] F. Mansour, R.M. Dimeo, H. Peemoeller, *Phys. Rev* E **66**,41 (2002).

[25] K.A. Dill., T.M. Truskett., V. Vlachy., B.H.-Lee., *Ann. Rev. Biophys.* **34**, 173 (2005).

[26] F. Franks., "*Water A Comprehsive Treatise Vol. 3* 301-399, Plenum Press, New-York (1973).

[27] R. Holly, H. Peemoeller, C. Choi, M. Pintar, *J. Chem. Phys.* **108**, 4183 (1998).

[28] J. Liang, Masters Thesis, University of Waterloo (2006).

[29] X.Z. Li., B. Walker., A. Michealides., *PNAS* **108**, 6369 (2011).

[30] B.S. Gonzalez., E.G. Noya., C. Vega., *J. Phys. Chem.* **114**, 2484 (2010).

[31] V. Osteroverkhov, G. Waychunas, Y. Shen. *Phys. Rev.* **94**, 046102 (2005).

[32] S. Takahara, M. Nakano, S. Kittaka. *J. Am. Chem. B.* **103**, 5814 (1999).

[33] D. Hwang, S. Sinha, C-Y. Cheng, T-Y. Yu, L. Huang. *Phys. Chem.* B, **105**, 5713 (2001).

[34] J. Trebosc, J. Wiench, S. Huh, V. Liu, M. Pruski, *J. Am. Chem.* B **127**, 3057 (2005).

[35] A. Abragam,. *The Principles of Nuclear Magnetism*, Oxford University Press London (1961).

[36] I. Chuang, G.E. Maciel. *J. Phys. Chem. B* **101**, 3052 (1997).

[37] J. Yang, S. Meng, L. Xu, E. Wang. *Phys. Rev. B.* **71**, 035413 (2005)

[38] V. Turov, V. Brei, K. Khomenko, R. Leboda. *Micro. Meso. Materials* **23**, 189 (1998)

[39] H. Eckert, J. Yesinowski, L. Silver, E. Stopler. *J. Phys. Chem.* **92**, 2055 (1988).